Discovery of Novel PI3-Kinase δ Specific Inhibitors for the Treatment of Rheumatoid Arthritis: Taming CYP3A4 Time-Dependent Inhibition

Brian S. Safina,*[,†] Stewart Baker,[∥] Matt Baumgardner,[†] Paul M. Blaney,[‡] Bryan K. Chan,[†] Yung-Hsiang Chen,[†] Matthew W. Cartwright,[‡] Georgette Castanedo,[†] Christine Chabot,[†] Arnaud J. Cheguillaume,[‡] Paul Goldsmith,[∥] David M. Goldstein,[§] Bindu Goyal,[§] Timothy Hancox,[∥] Raj K. Handa,[‡] Pravin S Iyer,[§] Jasmit Kaur,[∥] Rama Kondru,[§] Jane R. Kenny,[†] Sussie L. Krintel,[‡] Jun Li,[†] John Lesnick,[†] Matthew C. Lucas,[§] Cristina Lewis,[†] Sophie Mukadam,[†] Jeremy Murray,[†] Alan J. Nadin,[‡] Jim Nonomiya,[†] Fernando Padilla,[§] Wylie S. Palmer,[§] Jodie Pang,[†] Neil Pegg,[∥] Steve Price,[‡] Karin Reif,[†] Laurent Salphati,[†] Pascal A. Savy,[‡] Eileen M. Seward,[‡] Stephen Shuttleworth,[∥] Sukhjit Sohal,[∥] Zachary K. Sweeney,[†] Suzanne Tay,[†] Parcharee Tivitmahaisoon,[§] Bohdan Waszkowycz,[‡] Binqing Wei,[†] Qin Yue,[†] Chenghong Zhang,[†] and Daniel P. Sutherlin[†]

[†]Genentech, Inc., 1 DNA Way, South San Francisco, California 94080, United States
[‡]Argenta Discovery, 8/9 Spire Green Centre, Flex Meadow, Harlow CM19 5TR, United Kingdom
[§]Roche Research Center, 340 Kingsland Street, Nutley, New Jersey 07110, United States
[∥]Piramed Pharma, 957 Buckingham Avenue, Slough, Berks SL1 4NL, United Kingdom

Ⓢ Supporting Information

ABSTRACT: PI3Kδ is a lipid kinase and a member of a larger family of enzymes, PI3K class IA(α, β, δ) and IB (γ), which catalyze the phosphorylation of PIP2 to PIP3. PI3Kδ is mainly expressed in leukocytes, where it plays a critical, nonredundant role in B cell receptor mediated signaling and provides an attractive opportunity to treat diseases where B cell activity is essential, e.g., rheumatoid arthritis. We report the discovery of novel, potent, and selective PI3Kδ inhibitors and describe a structural hypothesis for isoform (α, β, γ) selectivity gained from interactions in the affinity pocket. The critical component

of our initial pharmacophore for isoform selectivity was strongly associated with CYP3A4 time-dependent inhibition (TDI). We describe a variety of strategies and methods for monitoring and attenuating TDI. Ultimately, a structure-based design approach was employed to identify a suitable structural replacement for further optimization.
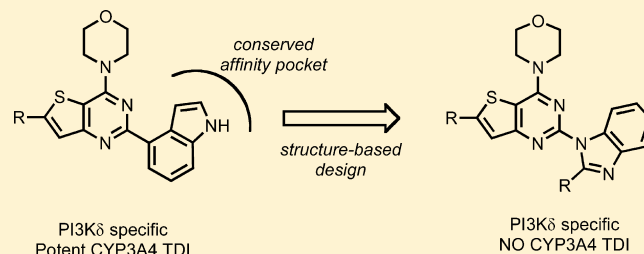
■ INTRODUCTION

Rheumatoid arthritis (RA) affects nearly 1% of the world population and places a significant burden upon society and patients.[1] RA is a debilitating autoimmune disorder, involving chronic inflammation of the synovial membrane lining the joints. Disease progression leads to pannus formation and eventually bone, cartilage, and ligament destruction resulting in pain, stiffness, and deformity. Disease-modifying antirheumatic drugs (DMARDs) remain the first line of treatment for the majority of patients due to low cost and ability to retard disease, especially at early onset. Treatment for RA has made significant advances over the last several decades, particularly since the introduction of biological therapies.[2] In recent years, targeted approaches such as TNF blockade, B cell depletion, costimulation blockade, and interleukin-6 receptor blockade have led to the control of symptoms and joint inflammation while retarding or halting joint damage all together. However, 50% of patients still do not respond to treatment with biologics

and only a small portion exhibit complete remission.[3] Furthermore, side effects tend to be serious and opportunistic infections may arise with fatal consequences.[4]

PI3Kδ is a lipid kinase and a member of a larger family of enzymes, PI3K class IA(α, β, δ), IB (γ), II, and III, which catalyze the phosphorylation of phosphatidylinositol-4,5-bisphosphate (PtdIns(4,5)P_2) (PIP2) to produce phosphatidylinositol-3,4,5-triphosphate (PtdIns(3,4,5)P_3) (PIP3), subsequently initiating a cascade of downstream events to modulate a variety of biological processes such as cell growth, proliferation, survival, and differentiation.[5] Class I PI3K isoforms exist as a heterodimer of one regulatory subunit (p85) with the corresponding catalytic subunit (p110α, p110β, p110δ). Activation of class IA enzymes occur through a tyrosine-kinase-dependent mechanism thought to involve

growth factors and cytokine receptors. Class IA PI3Ks have been implicated most notably in cancer and are ubiquitously expressed, with the exception of PI3Kδ, which is mainly expressed in leukocytes, where in B cells it is activated downstream of the B cell receptor.[6] Studies using mice with dominant negative mutants of PI3Kδ suggest that PI3Kδ plays a critical, nonredundant role in B cell receptor mediated signaling.[7] The role of B cell signaling in RA has been demonstrated by the efficacy of the B cell depleting CD20-specific monocolonal antibody rituximab[8] and in a variety of arthritis animal models.[9] Thus, targeting inhibition of PI3Kδ with a small-molecule inhibitor provides an attractive opportunity to treat rheumatoid arthritis. Specificity for PI3Kδ is desired because the ubiquitously expressed PI3K isoforms, α and β, have been shown to result in embryonic lethality in knockout mice and are thought to play essential roles in insulin action and platelet aggregation.[10] In contrast, genetic ablation of PI3K isoforms δ and γ in mice yield healthy and viable animals, with differences mainly in immune response.[10] PI3Kγ, also considered to be a target for the treatment of inflammatory diseases,[11] has not been shown to play a prominent role in B-cell function.

Previously reported ATP-competitive PI3Kδ specific inhibitors[12] have been shown to bind to p110δ by inducing an allosteric "specificity" pocket.[13] We describe a second unique class of ATP-competitive PI3Kδ specific inhibitors that bind in the affinity pocket and are derived from the morpholinyl thienopyrimidine scaffold (Figure 1).[14,19] This novel class of
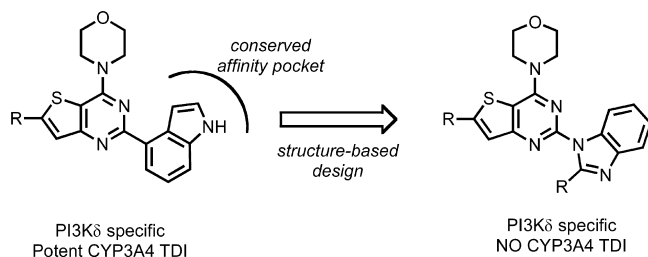

Figure 1. Discovery of the benzimidazole class of PI3Kδ specific inhibitors, free of CYP3A4 TDI.

inhibitors features an indole pharmacophore interacting with the conserved affinity pocket that is essential for high δ specificity. However, upon further profiling of compounds in this class, CYP3A4 time-dependent inhibition (TDI) was discovered, which led to unacceptable predictions for clinical drug–drug interactions (DDI).

Evaluating the DDI risk for NMEs is especially important in the treatment of chronic, nonlife-threatening diseases, such as rheumatoid arthritis, where the majority of patients are being treated with polypharmacy.[15] Early monitoring of CYP3A4 TDI and the potential of DDI in the drug discovery process has become critical for the identification of promising clinical candidates.[16] Reversible or mechanism-based inactivation of CYP3A4 can have significant consequences given that over half of the marketed drugs are metabolized by this enzyme. Moreover, mechanism-based inactivation suggests that metabolism results in the formation of a reactive metabolite capable of conjugating biomolecules which may result in idiosyncratic toxicity.[17] In this manuscript, we report the discovery of novel, potent, and selective benzimidazole containing PI3Kδ inhibitors that were discovered during our efforts to eliminate time-dependent CYP3A4 inhibition.

Synthesis. Compounds **1**−**39** (Scheme 1) were prepared from aldehyde **31**.[19] Intermediates **32**−**37** were derived from a reductive amination with the corresponding amine to yield six distinct aryl chloride intermediates (see Supporting Information). Several methods were employed to further functionalize aryl chloride intermediates **32**−**37**. Compounds **12**−**14**, **16**, **18**, and **21** proceeded through stannane intermediates **38**−**39** to afford the heteroaryl Stille coupling products. Compounds **1**−**2**, **4**−**11**, **15**, **17**, **19**−**20**, and **22**−**24** were constructed from either Suzuki couplings with boronic ester/acid partners or sodium hydride mediated nucleophilic additions in concentrated hydrochloric acid. Finally, compounds **25**−**30** were accessed through Buchwald couplings or stepwise benzimidazole construction via 1,2-diaminobenzene and concentrated hydrochloric acid followed by dehydrative mediated ring closure.

■ RESULTS AND DISCUSSION

Biochemical potencies for PI3K isoforms (α, β, δ, γ) were determined using a competitive fluorescence polarization assay measuring PI3K mediated formation of PIP3. Time-dependent inhibition was evaluated by employing two in vitro assays. Initial screening was through a high throughput "IC$_{50}$-shift" dilution assay[18] and was carried out by preincubating analogues (30 min) in human liver microsomes ($\pm$NADPH) and using CYP specific probe metabolite formation via LC-MS/MS to assess TDI risk. The assay reports a TDI-IC$_{50}$ (or the shifted IC$_{50}$ value following preincubation with NADPH) and a % change in AUC of the two $\pm$ NADPH inhibition curves. More detailed assays were performed to quantify the kinetic parameters k_{inact}, maximum rate of enzyme inactivation, and K_I, concentration supporting half the k_{inact}. TDI-IC$_{50}$ has been shown to strongly correlate with k_{inact}/K_I ratio,[18] thus we report TDI-IC$_{50}$ for key structure−activity relationships. Cellular potencies, detecting pAKT(S473), were determined using an Ri-1 cell line with added human serum albumin (HSA) and α-1-acid glycoprotein (AAG).

Comparing a set of indole and indazole-containing analogues (Table 1) provided pertinent clues to the origins of both PI3Kδ specificity and CYP3A4 TDI. Indole-containing analogues **1** and **2**, differing only in the piperazine substituent, were found to possess potent CYP3A4 TDI and ranged in α/δ selectivity from 22- to 129-fold. In contrast, replacement of the indole moiety with an indazole in compounds **3** (GDC-0941)[19] and **4** resulted in a reduction of PI3Kδ specificity (α/δ = 1- and 9-fold, respectively) along with no observed CYP3A4 TDI. These comparisons led us to hypothesize that the indole moiety was a key contributor to high δ specificity and also responsible for CYP3A4 TDI. Moreover, piperazine substitution seemed to act synergistically with the indole moiety in increasing p110δ specificity, which proved to be a critical observation for future optimization.[20]

Residues within the ATP-binding site and affinity pocket are highly conserved among all four isoforms (α, β, δ, γ) of class I PI3K lipid kinases. However, several key residue differences do exist. The difference in residues lying above the conserved tryptophan residue is notable (Figure 2, Trp760, PI3Kδ numbering). PI3Kδ contains a small threonine residue Thr750 which creates a surface we refer to as the tryptophan shelf. On the other hand, this residue is an arginine residue in PI3Kα, and a lysine residue in PI3Kβ and PI3Kγ, and the "shelf" is occluded. Above the hydrophobic region II lies the hinge region where the morpholine ring makes a vital contact

Scheme 1. Synthesis of Compounds 1−39[a]
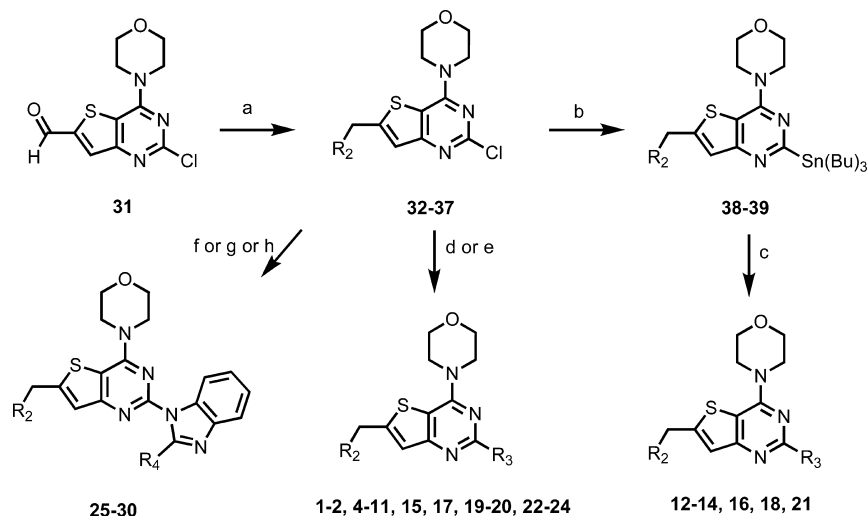
[a]Reagents and conditions: (a) amine, 1,2-DCE, Na(OAc)$_3$BH, 46−95%; (b) (Bu$_3$)$_2$Sn$_2$, PdCl$_2${PtBu$_2$(Ph-p-NMe$_2$)}$_2$, dioxane, microwave, 140−160 °C, 20 min, 54%; (c) aryl bromide, CuI, Pd(PPh$_3$)$_4$, THF, microwave, 140 °C, 20 min, 9−63%; (d) boronic acid/ester, Pd(PPh$_3$)$_2$Cl$_2$, NaHCO$_3$, H$_2$O, CH$_3$CN, microwave, 130−150 °C, 15−30 min, 26−83%; (e) indazole/indole, 0 °C, NaH, DMF, 30 min then 150 °C, 1 h, 27−49%; (f) benzimidazole, Pd$_2$(dba)$_3$, XPhos, Cs$_2$CO$_3$, DMF, microwave, 150 °C, 30 min, 42%; (g) benzimidazole, concd HCl, 1,4-dioxane, microwave, 150 °C, 40 min, 37−63%; (h) (i) 1,2-diaminobenzene, concd HCl, 1,4-dioxane, 90 °C, 3d, (ii) triethylorthoformate, 150 °C, 6 h, 26%.

Table 1. Inhibition of PI3Kα,β,δ,γ and CYP3A4-TDI for Indole and Indazole Containing Compounds 1−4

Compound	R$_1$	X	IC$_{50}$ (nM) PI3K-δ	fold selectivty α/δ	β/δ	γ/δ	Evidence of TDI
1		CH	1.8	129	104	1444	YES
2		CH	1.7	22	25	268	YES
3 (GDC-0941)		N	3.0	1	11	22	NO
4		N	3.1	9	54	153	NO

to Val828 and the affinity pocket where the indole moiety makes critical interactions[12] (vide infra). On a practical note, PI3Kδ specific inhibitors cocrystallized in the PI3Kγ isoform require additional modeling of the bound ligand in the context of a PI3Kδ homology structure. Nonetheless, the thienopyrimidine core serves as a good template for projecting substituents toward the tryptophan shelf and affinity pocket, setting the stage for further optimization of p110δ specificity.

The increase in PI3Kδ specificity resulting from a single-point replacement of a nitrogen atom with a methine group demanded further analysis of the ligand−protein interactions. Whereas our understanding of selectivity derived from the

tryptophan shelf was supported by isoform residue differences, the indole and indazole moiety both interacted with the *conserved* affinity pocket. Previous reports[19b] of the cocrystal structure containing **3** in PI3Kγ suggested that the indazole 2-nitrogen participates in a hydrogen bond with the phenol of Tyr867 and the indazole NH forms an interaction with Asp841 (Figure 3a). We theorized that the gain in selectivity resulting from the replacement of an indazole with an indole could be attributed to removing the strong hydrogen bonding interaction of **3** with Tyr867 and replacing it with a methine group (Figure 3b). Given that the residues in the affinity pocket are conserved throughout the class I isoforms, the precise consequences of this subtle hydrogen bonding reorganization is not fully understood. We hypothesized, the effect of disrupting the hydrogen bond with Tyr867 must radiate and extend past the conserved affinity pocket, resulting in undesirable conformational changes for the antitargets (α, β, γ), thereby providing PI3Kδ specificity. This hypothesis laid the foundation for future design of novel indole replacements.

While replacing the indazole unit with an indole moiety led to improvements in specificity, dramatic differences in time-dependent CYP3A4 inhibition were also observed. As previously mentioned, initial structure−activity relationships implicated the indole ring as the functional group responsible for CYP3A4 TDI, independent of the N-piperazine substitution (Table 1). Compound **5**, Table 2, exhibited good affinity for PI3Kδ (3 nM) and excellent (>100-fold) isoform selectivity (α/δ = 194, β/δ = 102, γ/δ = 1877) along with a clean profile across a broad kinase panel (Invitrogen 240 kinases @ 1 μM). Compound **5** was selected for further evaluation and was found to inactivate CYP3A4 with an IC$_{50}$ of 1.5 μM when preincubated (30 min) with human liver microsomes. Further measurement of the maximal inactivation rate (k_{inact} = 0.074 min^{-1}) and inactivator potency (K_I = 6.59 μM) yielded a k_{inact}/K_I ratio of 11.0 mL/min/μmol, confirming time-dependent inhibition of CYP3A4. DDI assessment was performed using Symcyp, a population-based ADME simulator.[21] Simulations were performed where **5** (500 mg BID for 5 days) was
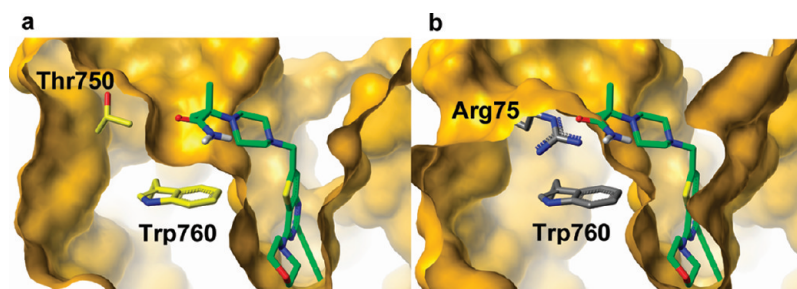
Figure 2. Model of structure **12** (structure shown in Table 3) bound to (a) PI3Kδ (PDB entry 2WXP), highlighting the tryptophan shelf and (b) PI3Kα, highlighting the tryptophan shelf being occluded by Arg75.
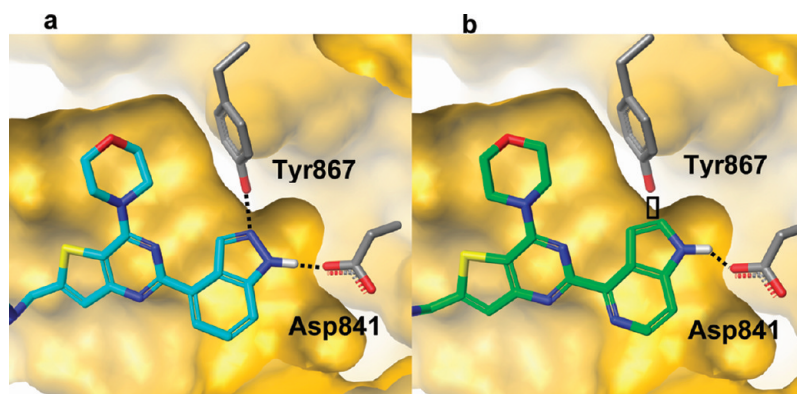

Figure 3. Model comparing indazole and indole interactions in the affinity pocket of PI3Kδ. (a) Compound **3** highlighting interactions with Tyr867 and Asp841. (b) Compound **12**, lacking a hydrogen bond acceptor, resulted in greater PI3Kδ specificity.

Table 2. Time-Dependent Inhibition of CYP3A4 in Human Liver Microsomes and Pharmacokinetics in Male HW Rats, 0.5 mpk iv and 2 mpk po for Compounds 5 and 6

| compd | TDI-CYP3A4(t) | | | | %F | CL (mL/min/kg) | V_{dss} (L/kg) | $T_{1/2}$ |
	IC_{50} (μM)	k_{inact} (1/min)	K_I (μM)	k_{inact}/K_I				
5	1.5	0.074	6.6	11	75.2	31.3	2.38	1.48
6	7.0	0.048	78	0.60	75.5	25.2	2.76	1.60

coadministered with a single dose of midazolam (15 mg, day 5), resulting in predicted 20-fold increase in midazolam AUC. Compounding matters further, cytochrome P450 (CYP) phenotyping indicated that **5** was predominately metabolized by CYP3A4 and would consequently suffer from autoinhibition and have a dramatic effect on its own clearance upon multiple dosing. As a result of these findings, **5** was deemed unsuitable for further development and we began to develop a strategy to monitor and reduce TDI for indole-containing analogues.

In search of a structural hypothesis to guide target design and identify reactive metabolites, we turned to metabolite identification studies (MetID). Compound **5** was incubated in human and rat liver microsomes in the presence of NADPH, UDPGA, and GSH, followed by fragment analysis by mass spectrometry (Figure 4). The major metabolites were found to result from the oxidation of the morpholine ring (1.6% human,
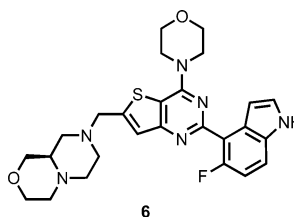
5.2% rat (M1 and M2)), followed by oxidation of the morpholino thienopyrimidine core and indole moiety (1.3% human, 1.4% rat (M3)). A small fraction of glucuronide conjugate of an oxidative metabolite was also observed (0.2%, M4) in both human and rat liver microsomes. Glutathione conjugate was not observed in in vitro MetID, but in vivo, a minimal amount (<100 fold to parent) of glutathione conjugation to M3 was identified in rat bile (30 mg/kg PO).

Struck by the lack of metabolism of the piperazine group in compound **5**, we speculated that we might redirect metabolism from the thienopyrimidine core and indole ring (M2, Figure 4) to the piperazine in order to diminish TDI.[22] Compound **6** (Table 2), possessing a fused morpholino piperazine group, was identified as a moderate affinity inhibitor of PI3Kδ (9 nM), which also possessed moderate (10−100-fold) isoform selectivity (α/δ = 42, β/δ = 69, γ/δ = 806). Upon comparison

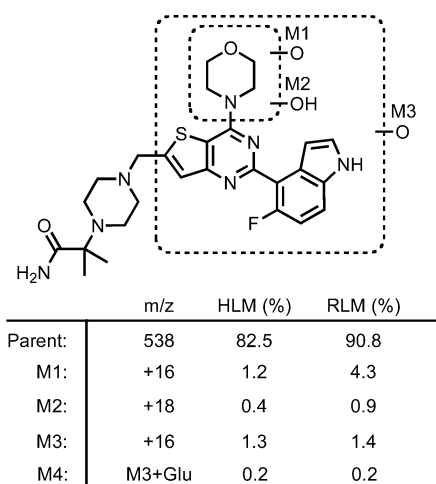|	m/z	HLM (%)	RLM (%)
Parent:	538	82.5	90.8
M1:	+16	1.2	4.3
M2:	+18	0.4	0.9
M3:	+16	1.3	1.4
M4:	M3+Glu	0.2	0.2

Figure 4. MetID of compound **5** in liver microsomes.

of metabolites of compounds **5** and **6** in rat and human liver microsomes (Figure 5), it was found that metabolism was
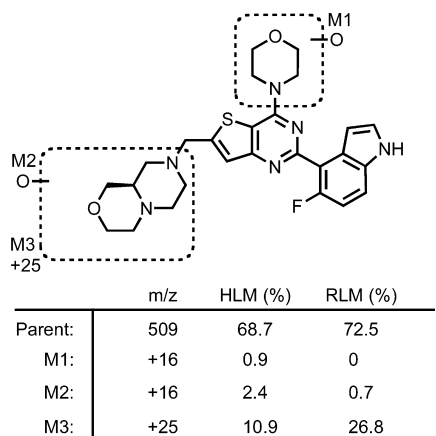

	m/z	HLM (%)	RLM (%)
Parent:	509	68.7	72.5
M1:	+16	0.9	0
M2:	+16	2.4	0.7
M3:	+25	10.9	26.8

Figure 5. MetID of compound **6** in liver microsomes.

directed away from the thienopyrimidine core and indole moiety and predominantly toward the fused morpholino piperazine group, M2 (2.4% human, 0.7% rat) and M3 (10.9% human, 26.8% rat).

In kinetic measurements, the ratio of k_{inact}/K_I for **6** (Table 2) indicated that it was 18-fold less potent than for **5**, which further strengthened our correlation between TDI IC$_{50}$ and k_{inact}/K_I and allowed us to use TDI IC$_{50}$ as a primary optimization parameter. Further comparisons of the in vivo rat pharmacokinetic profile for the two compounds (Table 2) showed that the clearance (~30 mL/min/kg) and bioavailability (75%) were equivalent. The fused morpholino piperazine group was successful in diverting metabolism away from the thienopyrimidine core and indole ring while maintaining moderate in vivo clearance and reducing CYP3A4 TDI.

Ultimately, the strategy to redirect metabolism away from the indole, while maintaining high selectivity and permeability, proved restrictive and modification of the indole heterocycle was deemed necessary. This presented a challenge in that the unique specificity for PI3Kδ resulted largely from the indole (vide supra). Cytochrome P450-catalzyed oxidative metabolism of the indole ring has been extensively reported in the

literature.[23] Consistent with observations from MetID studies (compound **5**, Figure 4) in which we observed oxidation (M3) followed by glucuronidation (M4), we focused on several possible sites for cytochrome P450 mediated oxidation of the indole ring to serve as the foundation for target design.

Depending upon substitution and/or electronic effects, the indole ring can undergo a myriad of transformations potentially leading to reactive metabolites capable of inactivating cytochrome P450 (Figure 6). Mechanistically, cytochrome
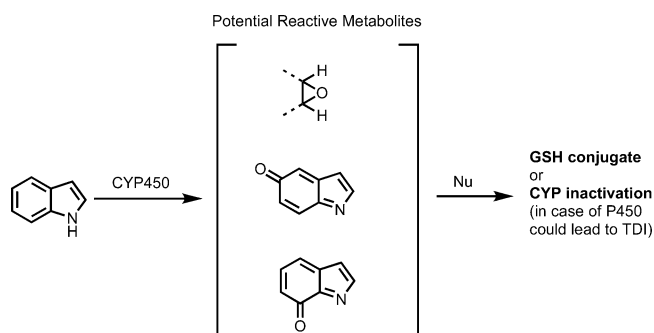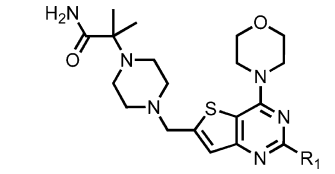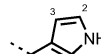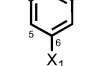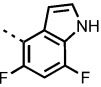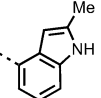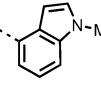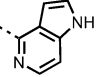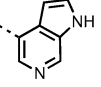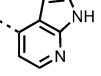

Figure 6. Reactive metabolites formed from CYP450 mediated oxidation of the indole ring, potentially causing CYP3A4 TDI.

P450 oxidation is thought to take place through several reaction manifolds involving heme iron and oxygen.[24] All of the proposed reactive metabolites are susceptible to nucleophilic addition, and we postulated that blocking this metabolism would lead to a reduction in CYP3A4 TDI.

Thus, exploration began by decorating the indole ring in order to block possible sites of aromatic hydroxylation (C5−C7 positions) without disrupting the C-2/3 position of the indole ring critical for δ specificity and affinity. Compounds **7−9** (Table 3) demonstrate that substitution at C-5, C-6, and C-7 positions of the indole ring had little impact on PI3Kδ potency and isoform selectivity. Unfortunately, there was also no improvement in TDI. Moving toward the C-2 and C-3 positions of the indole ring, we examined the consequence of methylating the C-2 position (Table 3, compound **10**), further perturbing our postulated interaction with Tyr867. Interestingly, the increased size and lipophilicity of the methyl group was well tolerated, judged by the resulting potency and selectivity, further reinforcing our Tyr867 selectivity hypothesis. Methylation of the indole nitrogen gave compound **11** which possessed no TDI and thus proved to be very informative, further implicating the indole as a reactive metabolite progenitor. More specifically, these results led us to speculate that N-hydroxylation could be responsible for CYP inactivation, although the exact mechanism and structure of the reactive metabolite responsible remained unclear. Regardless, disrupting this key N−H interaction ablated PI3Kδ potency and thus served no practical utility. Analogues containing C-3 substituents were not synthesized because computational analysis predicted unfavorable torsional angles (data not shown) between the indole ring and bicycle core and would have a detrimental impact on potency and/or selectivity. Our attention was then turned to a set of azaindole analogues (Table 3, compounds **12−14**) designed to reduce calculated lipophilicity (cLogP), thereby warding off metabolism and/or altering the ring electronics and attenuating CYP related reactivity. Gratifyingly, 5-azaindole analogue **12** resulted in no TDI (IC$_{50}$ >10 uM) while both 6- and 7-azaindoles (**13** and **14**)

Table 3. Inhibition of PI3Kα, β, δ, γ, and CYP3A4 Time-Dependent Inhibition for Compounds 7−14

Compound	R$_1$	IC$_{50}$ (nM) PI3K-δ	fold selectivty α/δ	β/δ	γ/δ	IC$_{50}$ (μM) TDI-CYP3A4(t)
7: X$_1$=F		0.48	77	80	566	0.51
8: X$_1$=CN		3.2	208	275	691	1.2
9		6.0	96	137	350	0.60
10		1.1	122	101	715	<0.10
11		134	18	75	75	>10
12		3.5	86	46	2831	>10
13		0.67	41	40	243	3.2
14		2.3	30	103	81	<0.10

resulted in moderate to strong TDI. This trend, increasing TDI potency, appeared to correlate with the reduction in calculated pK_a values for azaindoles **12** (8.77), **13** (7.44), and **14** (4.52).[25] Unfortunately, the 5-azaindole **12** and subsequent analogues were unsuitable for progression due to generally poor cellular potency, low permeability, and only moderate isoform selectivity.

After an extensive effort to minimize TDI while preserving the indole ring, we undertook the challenge of finding a suitable replacement group, which was TDI free and had suitable potency and α/δ isoform selectivity to serve as a starting point for further optimization. Guided by our structurally driven hypothesis for PI3Kδ specificity, we set out to synthesize a variety of analogues exploring diverse indole replacements capable of filling the affinity pocket while minimizing strong hydrogen bonding interactions with Tyr867. Several key design elements were extracted from a more detailed analysis of the indole bound in the affinity pocket, Figure 7.

The affinity pocket encapsulating the indole moiety was generally lipophilic and displayed additional space to accommodate substituents for further gains in affinity. We also attempted to match ground-state conformations with bound conformations by targeting indole replacements with calculated torsional angles similar to that observed in the X-ray cocrystal structure of **12** (torsional angle = 30°). In addition to probing interactions with Tyr867, we were cognizant of Lys779 and the potentially favorable opportunities that it presented. In search of a δ specific pharmacophore, we primarily monitored α/δ selectivity, which tended to be a good predictor for overall isoform selectivity. We selected the dimethylamino piperidine side chain (Table 4) because it was suitable for making direct analogue comparisons in α/δ selectivity, exemplified by fluoroindole **15** (δ = 1.8 nM, α/δ = 226). Indolinone **16** challenged the Tyr selectivity hypothesis by attempting to engage the phenol with a hydrogen bond acceptor (HBA), which indeed translated into diminished selectivity (α/δ = 8) and overall lower affinity (δ = 41 nM). Drastic simplification to an o-toluene moiety resulted in **17**, which had surprisingly good selectivity (α/δ = 98) and moderate affinity for PI3Kδ. Predictably, however, lipophilicity was greatly increased and cellular potency was severely affected. Further modifications of **17** revealed a sharp SAR trend, and thus this series was deemed unsuitable for a focused optimization effort.

Indole-like mimics, which preserved the general 6,5-heterocyclic framework, such as imidazopyridine **18**, were instructive, because the sp^2 C−H subunit pointing toward the tyrosine was preserved. Replacing the indole's N−H (HBD) with a hydrogen bond acceptor (HBA) in **18** highlights the important interactions with the Asp841 water network. Moreover, compounds such as **18**, which contain a H-bond acceptor in place of the H-bond donor of the indole were
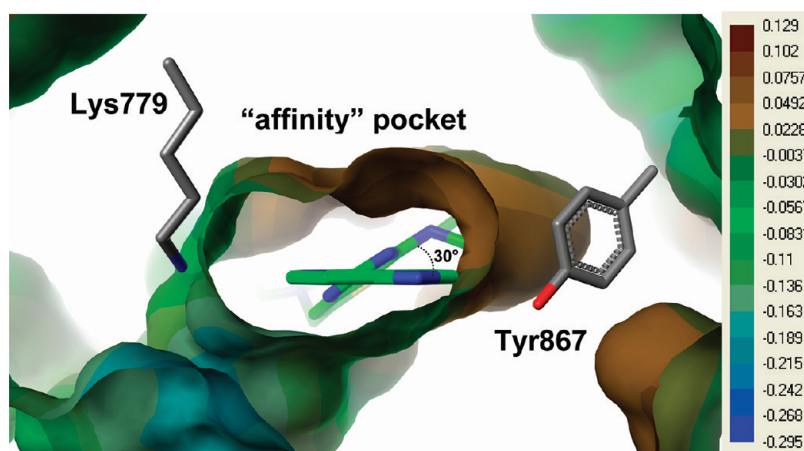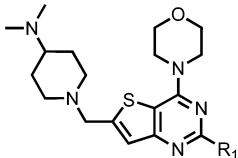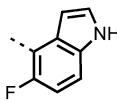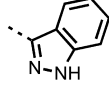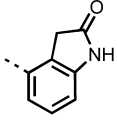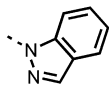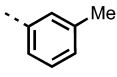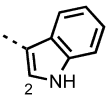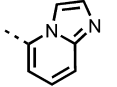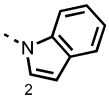

Figure 7. Analysis of the affinity pocket in the X-ray cocrystal structure of indole **12** (PI3Kγ). Lipophilic (brown) and hydrophilic (blue).[26].

Table 4. Inhibition of PI3Kα and δ, pAKT Ri-1 Inhibition for Compounds 15–26

Compound	R_1	IC_{50} (nM)		IC_{50} (μM)	Compound	R_1	IC_{50} (nM)		IC_{50} (μM)
		PI3K-δ	α/δ	pAKT Ri-1			PI3K-δ	α/δ	pAKT Ri-1
15		1.8	226	0.029	21		9.8	65	ND
16		41	8	3.4	22		16	39	3.2
17		12	98	1.3	23		5.6	88	ND
18		27	21	0.18	24		10	54	0.42
19		29	144	2.0	25		23	14	0.97
20		2.4	94	3.8	26		2.7	29	0.374

generally less potent and ultimately had diminished PI3Kδ affinity and specificity, presumably due to nitrogen lone pair-to-Asp repulsion. Similarly, isoquinoline **19** possessed low δ affinity (29 nM) but its high α/δ selectivity (144 fold) warranted exploration of heteroaromatic bicycles and phenyl groups properly oriented within the affinity pocket.

Modeling suggested that a variety of 5,6-heteroaromatic systems (compounds **20–26**) could occupy the affinity pocket and provide sufficient potency and selectivity. In general, all of the analogues provided moderate α/δ selectivity, which was acceptable, especially as a starting point. Several additional key features, however, played a role i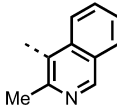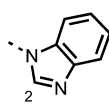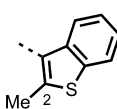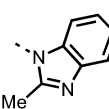n our selection of a suitable indole replacement. Heterocycles capable of further functionalization at the 2-C position (i.e., **23** and **24**, **25**) were investigated primarily for their ability to provide additional handles for optimization. We envisioned that substitution at this position would provide opportunities to make favorable protein interactions and/or adjust the torsional angles of our inhibitors. For example, 2-Me substituted benzimidazole **26** gave rise to a 10-fold improvement in p110δ affinity over the unsubstituted (2-H) benzimidazole **25**. When deciding which heterocycle to subject to further SAR, we chose to avoid highly lipophilic and potentially toxicophoric groups such as thiophene **20** and indoles **23** and **24**, capable of CYP mediated N-hydroxylation. We favored benzimidazole **25** for its low cellular shift (pAKT-Ri-1/PI3Kδ = 42-fold), which compared favorably to the indole class of analogues, (e.g., compound **15**,

pAKT-Ri-1/PI3Kδ = 16-fold). From a structural perspective, the affinity pocket seemed to accommodate a wide array of ligand diversity, but the benzimidazole moiety was also uniquely positioned to forge favorable interactions with Lys779 (Figure 8), similar to what was observed with azaindole **12**. Ultimately, the benzimidazole moiety possessed all of these unique characteristics required for progression.
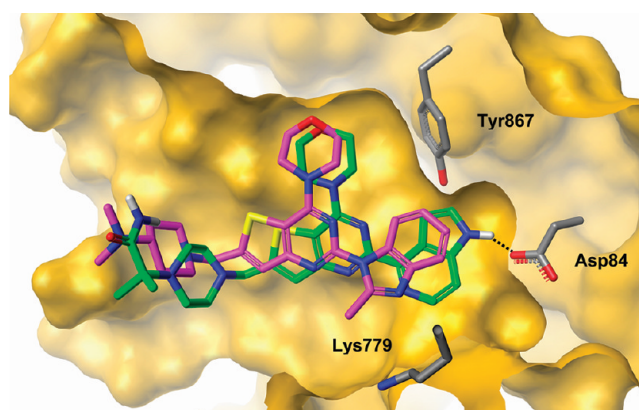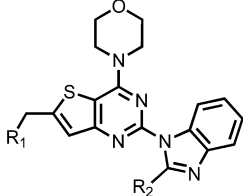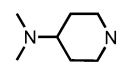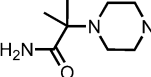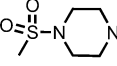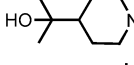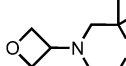

Figure 8. Overlay of cocrystal stuctures in PI3Kγ (compounds **26**, pink, and **12**, green) comparing binding modes of indole and benzimidazole containing analogues.

Table 5. Inhibition of PI3Kα, β, δ, γ, CYP3A4 TDI and pAKT Ri-1 for compounds 26−30

Compound	R$_1$	R$_2$	IC$_{50}$ (nM) PI3K-δ	fold selectivty α/δ	β/δ	γ/δ	IC$_{50}$ (μM) pAKT Ri-1	IC$_{50}$ (μM) TDI-CYP3A4(t)
26		Me	2.7	29	252	233	0.40	>10
27		Me	4.3	17	111	134	ND	>10
28		Et	4.3	2	12	14	0.079	>10
29		Et	5.3	19	78	115	0.116	>10
30		Et	2.3	50	815	112	0.102	>10

While monitoring for CYP3A4-TDI, we found that the dimethylamino piperidine side chain, possessing a very high pK_a (∼10), tended to reduce TDI, possibly masking it from compounds 16−26 (e.g., indole 15 exhibited CYP3A4-TDI = 9.1 μM). Thus, to further strengthen our belief that a suitable TDI-free indole replacement was being chosen, a set of benzimidazole analogues, all possessing groups with reduced basicity, were synthesized 27−30 (Table 5) all confirming a TDI-IC$_{50}$ >10 μM. In addition, the cellular potency was within the desired range (<200 nM) for the majority of analogues (i.e., 28−30). Benzimidazole compound 27 possessed a desirable cLogP (2.3) and moderate predicted human liver microsome stability (10 mL/min/kg), equivalent to indole compound 5 (10 mL/min/kg).

X-ray crystallographic analysis of benzimidazole 26 revealed a shift in binding mode, compared to azaindole 12 (Figure 8, overlay of compounds 26 and 12). The single point contact of the morpholine hinge binder allowed for a clockwise pivot of the ligand, affording new opportunities and interactions in both the affinity pocket (e.g., Lys779) and "tryptophan" shelf. Reoptimization of the central heterocycle and highly basic functionality of the dimethylamino piperazine group was also in order. To this end, introduction of a *gem*-dimethylpiperazine moiety (compound 30), designed to fill the nearby tryptophan shelf, led to excellent selectivity over PI3Kβ (β/δ = 815) and moderate selectivity over PI3Kγ and α (γ/δ = 112 and α/δ = 50). Thus having fulfilled all of our requirements (reduced TDI, excellent potency and moderate specificity), the benzimidazole class of indole replacements was perfectly positioned for further optimization.

CONCLUSION

A novel class of PI3Kδ specific benzimidazole inhibitors has been discovered through our efforts to reduce CYP3A4 time-dependent inhibition of indole containing analogues. Initial SAR and metabolism identification studies with compound 5 implicated the indole ring as causing CYP3A4 TDI and laid the foundation germane to constructing a hypothesis. We successfully implemented several strategies such as installing metabolic soft spots to divert metabolism, blocking potential sites of metabolism leading to reactive metabolite formation and modifying physiochemical properties (pK_a and cLogP) to reduce TDI. Ultimately, identification of an indole-containing compound with reduced TDI combined with acceptable potency, selectivity, and overall favorable drug-like properties was elusive.

Through the use of cocrystal structures in PI3Kγ and structure-based design, our understanding of the principles driving PI3Kδ potency and specificity allowed for the exploration of several novel pharmacophores to replace the indole moiety and test our selectivity hypothesis. On the basis of the discovery of several novel, potent PI3Kδ specific indole replacements, we selected the benzimidazole group for its favorable drug-like properties (i.e., metabolic stability, cellular potency, substitution, and lack of CYP3A4 TDI). Further cocrystal structural analysis of benzimidazole analogues exhibited a distinct pivot about the morpholine hinge, in contrast to the indole-containing inhibitors, providing further opportunities for the development of PI3Kδ specific benzimidazole inhibitors in rheumatoid arthritis, details of which will be described in due time.

EXPERIMENTAL SECTION

μm All solvents and reagents were used as obtained. ^{1}H NMR spectra were recorded with a Bruker Avance DPX400 spectrometer or a Varian Inova 400 NMR spectrometer and referenced to tetramethylsilane. Chemical shifts are expressed as δ units using tetramethylsilane as the internal standard (in NMR description: s, singlet; d, doublet; t, triplet; q, quartet; m, multiplet; br, broad peak). All coupling constants (*J*) are reported in hertz. Mass spectra were measured with a Finnigan SSQ710C spectrometer using an ESI source coupled to a Waters 600MS HPLC system operating in reverse mode with an X-bridge phenyl column of dimensions 150 mm × 2.6 mm, with 5 μm sized particles. Analytical purity was >95% unless stated otherwise. The following analytic method was used, unless stated otherwise, HPLC-

Agilent 1200, water with 0.05% TFA, acetonitrile with 0.05% TFA, Agilent Zorbax SD-C18, 1.8 μM, 2.1 mm × 30 mm, 40 °C, 3−95%B in 8.5 min, 95% in 2.5 min, 400 μL/min, 220 nm and 254 nm, equipped with Agilent quadrupole 6140, ESI positive, 110−800 amu. Microwave reactions were performed using a Biotage initiator reactor. Compound **3** and intermediates **31** and **33** have been previously described.[19] Procedures for unreported compounds and intermediates **32−39** are described in the Supporting Information.

2-(4-((2-(1*H*-Indol-4-yl)-4-morpholinothieno[3,2-d]-pyrimidin-6-yl)methyl)piperazin-1-yl)-2-methylpropanamide (1). A 20 mL microwave vial was charged with a suspension of 2-(4-((2-chloro-4-morpholinothieno[3,2-*d*]pyrimidin-6-yl)methyl)-piperazin-1-yl)-2-methylpropanamide (**32**) (see Supporting Information for procedure) (0.293 g, 0.67 mmol), 4-(4,4,5,5-tetramethyl-[1,3,2]dioxaborolan-2-yl)-1*H*-indole (0.21 g, 0.87 mmol), cesium carbonate (0.472 g, 1.34 mmol), and Pd(PPh$_3$)$_4$ (0.077 g, 0.067 mmol) in dioxane (8 mL) and water (2 mL). The reaction mixture was heated in a microwave for 15 min at 140 °C. The crude reaction mixture was loaded onto an SCX-2 cartridge, and the cartridge was washed with methanol; the product was eluted with 2N ammonia in methanol. The solution was concentrated, and the residue was further purified by chromatography (Si-PPC) using 0−5% MeOH in DCM as eluant. The fractions containing the product were concentrated in vacuo. The residue was crystallized from EtOH to give the product as a white crystalline solid (100 mg, 28%). ^{1}H NMR (CDCl$_3$) δ 8.71 (br s, 1H), 8.16 (d, J = 7.5, 1.0 Hz, 1H), 7.49−7.51 (m, 1H), 7.44 (dt, J = 8.0, 1.0 Hz, 1H), 7.35 (s, 1H), 7.25−7.30 (m, 2H), 7.09 (br d, J = 5.5 Hz, 1H), 5.65 (br d, J = 5.5 Hz, 1H), 4.07 (t, J = 4.0 Hz, 4H), 3.89 (t, J = 4.0 Hz, 4H), 3.81 (s, 2H), 2.50−2.64 (m, 8H), 1.22 (s, 6H). LCMS m/z [M + H]$^+$ 520.

4-(2-(1*H*-Indol-4-yl)-6-((4-(methylsulfonyl)piperazin-1-yl)-methyl)thieno[3,2-*d*]pyrimidin-4-yl)morpholine (2). The title compound was prepared from **33** in a manner similar to the Suzuki procedure described for compound **1** to give compound **2**. ^{1}H NMR (400 MHz, CDCl$_3$) δ 2.67−2.71 (4H, m), 2.81 (3H, s), 3.29−3.33 (4H, m), 3.89 (2H, s), 3.89−3.93 (4H, m), 4.08−4.12 (4H, m), 7.28−7.33 (m, 2H), 7.39 (s, 1H), 7.50 (d, J = 8.2 Hz, 1H), 7.53−7.54 (m, 1H), 8.19 (d, J = 8.0 Hz, 1H), 8.28 (br s, 1H). LCMS m/z [M + H]$^+$ 513.2. LCMS 30 min. CAD GRADIENT, 0.7 mL/min on Agilent 1200/G6140 system). Purity is 100% by UV 254.

2-(4-((2-(1*H*-Indazol-4-yl)-4-morpholinothieno[3,2-*d*]-pyrimidin-6-yl)methyl)piperazin-1-yl)-2-methylpropanamide (4). The title compound was prepared from **32** in a manner similar to the Suzuki procedure described for compound **1** to give compound **4** (40 mg, 40%). ^{1}H NMR (500 MHz, CDCl$_3$) δ 10.25 (s, br, 1H), 9.01 (s, 1H), 8.26 (d, 1H), 7.62 (m, 1H), 7.51 (m, 1H), 7.36 (s, 1H), 7.12 (m, 1H), 5.25 (m, 1H), 4.11 (m, 4H), 3.90 (m, 4H), 3.83 (s, 2H), 2.62 (s, br, 8H), 1.25 (s, 6H). RT: 1.94 min. LCMS m/z [M + H]$^+$ 521.1. Analytical LC-MS on an Agilent (1200/G6140) using a 1.8 μM, 2.1 mm × 30 mm ZORBAX SD-C18 analytical column, 40 °C, 400 μL/min, and H$_2$O/MeCN modified with 0.05% trifluoroacetic acid running a linear gradient from 3% MeCN to 95% MeCN in 10 min monitoring by UV wavelength 254 nm and ESI+ TIC MS showed 100% purity.

2-(4-((2-(5-Fluoro-1*H*-indol-4-yl)-4-morpholinothieno[3,2-*d*]-pyrimidin-6-yl)methyl)piperazin-1-yl)-2-methylpropanamide (5). The title compound was prepared from **32** and 1-(*tert*-butyldimethylsilyl)-5-fluoro-4-(4,4,5,5-tetramethyl-1,3,2-dioxaborolan-2-yl)-1*H*-indole (see Supporting Information for procedure) in a manner similar to the Suzuki procedure described for compound **1** to give compound **5** obtained as a white solid (77 mg, 78%). ^{1}H NMR (400 MHz, CD$_3$OD) δ 1.90 (s, 6H), 2.56−2.64 (m, 8H), 3.82 (m, 4H), 3.87 (m, 2H), 4.02 (m, 4H), 6.58 (dd, J = 0.8, 3.7, 1H), 6.95 (dd, J = 8.8, 11.0, 1H), 7.28 (s, 1H), 7.30 (s, 1H) and 7.41 (ddd, J = 0.8, 4.0, 8.8, 1H). RT: 7.44 min. LCMS m/z [M + H]$^+$ 538.4. Analytical LC-MS on an Agilent (1200/G6140) using a 1.8uM, 2.1 mm × 30 mm ZORBAX SD-C18 analytical column, 40 °C, 700 μL/min, and H$_2$O/MeCN modified with 0.05% trifluoroacetic acid running a linear gradient from 2% MeCN to 98% MeCN in 30 min monitoring by UV wavelength 254 nm and ESI+ TIC MS showed 100% purity.

(*R*)-8-((2-(5-Fluoro-1*H*-indol-4-yl)-4-morpholinothieno[3,2-*d*]pyrimidin-6-yl)methyl)octahydropyrazino[2,1-*c*][1,4]oxazine (6). A mixture of (*R*)-8-(2-chloro-4-morpholin-4-ylthieno[3,2-*d*]-pyrimidin-6-ylmethyl)octahydropyrazino[2,1-*c*][1,4]oxazine (**34**) (200 mg, 0.49 mmol), Cs$_2$CO$_3$ (318 mg, 0.98 mmol), 1-(*tert*-butyldimethylsilanyl)-5-fluoro-4-(4,4,5,5-tetramethyl-[1,3,2]-dioxaborolan-2-yl)-1*H*-indole (238 mg, 0.63 mmol), and tetrakis-(triphenylphosphine)palladium (56 mg, 0.05 mmol) in dioxane/water (8 mL/4 mL) was heated at 140 °C for 25 min in a microwave reactor. The resulting cooled mixture was loaded onto an SCX column, and the column was washed with DCM and methanol. The product was eluted with 2 M NH$_3$ in methanol, and the product fractions were concentrated in vacuo. The residue obtained was purified by column chromatography on silica using 1−10% 2 M NH$_3$ in EtOAc as eluant to give compound **6** as a yellow solid (207 mg, 83%). ^{1}H NMR (400 MHz, CDCl$_3$) δ 1.91 (m, 1 H), 2.36−2.47 (m, 4 H), 2.63−2.78 (m, 3 H), 2.95 (d, J = 8.6 Hz, 1 H), 3.25 (m, 1 H), 3.62−3.74 (m, 2 H), 3.81−3.89 (m, 7 H), 4.05 (t, J = 4.7 Hz, 4 H), 6.88−6.90 (m, 1 H), 7.05 (dd, J = 10.9, 8.8 Hz, 1 H), 7.28 (m, 1 H), 7.34−7.39 (m, 2 H) and 8.22 (br s, 1H). RT: 6.61 min. LCMS m/z [M + H]$^+$ 509.2. Analytical LC-MS on an Agilent (1200/G6140) using a 1.8uM, 2.1 mm × 30 mm ZORBAX SD-C18 analytical column, 40 °C, 400 μL/min, and H$_2$O/MeCN modified with 0.05% trifluoroacetic acid running a linear gradient from 3% MeCN to 95% MeCN in 10 min monitoring by UV wavelength 254 nm and ESI+ TIC MS showed 97% purity.

2-(4-((2-(6-Fluoro-1*H*-indol-4-yl)-4-morpholinothieno[3,2-*d*]-pyrimidin-6-yl)methyl)piperazin-1-yl)-2-methylpropanamide (7). The title compound was prepared from **32** in a manner similar to the Suzuki procedure described for compound **1** to give compound **7** as an off-white solid (95 mg, 65%). ^{1}H NMR (400 MHz, CDCl$_3$) δ 1.26 (s, 6H), 2.63 (m, 8H), 3.87 (s, 2H), 3.93 (t, J = 4.8, 4H), 4.10 (t, J = 4.8, 4H), 5.18 (br s, 1H), 7.10 (br s, 1H), 7.20 (dd, J = 1.1, 6.5, 1H), 7.32 (m, 1H), 7.38 (s, 1H), 7.56 (s, 1H), 8.99 (dd, J = 2.3, 8.8, 1H), 8.26 (br s, 1H). LCMS m/z [M + H]$^+$ 538.4.

2-(4-((2-(6-Cyano-1*H*-indol-4-yl)-4-morpholinothieno[3,2-*d*]-pyrimidin-6-yl)methyl)piperazin-1-yl)-2-methylpropanamide (8). The title compound was prepared from **32** in a manner similar to the Suzuki procedure described for compound **1** to give compound **8** as a cream solid (41 mg, 47%). ^{1}H (400 MHz, CDCl$_3$) δ 1.27 (s, 6H), 2.63 (m, 8H), 3.88 (s, 2H), 3.94 (t, J = 4.7, 4H), 4.11 (t, J = 4.7, 4H), 5.21 (br s, 1H), 7.12 (br s, 1H), 7.39 (s, 1H), 7.55 (t, J = 5.6, 1H), 7.69 (s, 1H), 7.82 (s, 1H), 8.47 (s, 1H), 8.60 (br s, 1H). LCMS m/z [M + H]$^+$ 545.4.

2-(4-((2-(5,7-Difluoro-1*H*-indol-4-yl)-4-morpholinothieno-[3,2-*d*]pyrimidin-6-yl)methyl)piperazin-1-yl)-2-methylpropa-namide (9). To a solution of 2-(4-((2-chloro-4-morpholinothieno-[3,2-*d*]pyrimidin-6-yl)methyl)piperazin-1-yl)-2-methylpropanamide (**32**) (66.06 mg, 0.1505 mmol) in acetonitrile (3 mL) in a microwave reaction vessel was added 1-(*tert*-butoxycarbonyl)-5,7-difluoro-1*H*-indol-4-ylboronic acid (89.4 mg, 0.301 mmol) (see Supporting Information for procedure), bis(triphenylphosphine)palladium(II) chloride (5.28 mg, 0.00752 mmol), and a 1 M solution of sodium carbonate (47.8 mg, 0.452 mmol) in water. The tube was sealed and heated at 130 °C under microwave irradiation for 30 min. The solvent was evaporated, and the residue was purified by column chromatography (Si-PPC, MEOH/DCM, gradient 0:100 to 20:80) followed by reverse phase HPLC (Phenomenex Gemini 5 μ C18, 20 mM triethylamine in water on a gradient of acetonitrile 70:30 to 40:60). LCMS (10 min run): RT 3.17 min, [M + H]$^+$ 556.2. ^{1}H NMR (400 MHz, DMSO-d_6) δ 11.77 (br s, 1H), 7.52−7.47 (m, 1H), 7.72−7.36 (m, 1H), 7.10−6.99 (m, 2H), 6.97−6.90 (s, 1H), 6.83−6.78 (m, 1H), 3.96−3.89 (m, 4H), 3.89−3.83 (br s, 2H), 3.80−3.73 (m, 4H), 2.67 (s, 1H), 2.34−2.31 (s, 1H), 2.30−2.27, m, 2H), 2.62−2.54 (m, 4H), 1.14−1.03 (m, 6H). Analytical LC-MS on an Agilent (1200/G6140) using a 1.8 μM, 2.1 mm × 30 mm ZORBAX SD-C18 analytical column, 40 °C, 400 μL/min, and H$_2$O/MeCN modified with 0.05% trifluoroacetic acid running a linear gradient from 3% MeCN to 95% MeCN monitoring by UV wavelength 254 nm and ESI+ TIC MS showed 100% purity.

2-Methyl-2-(4-((2-(2-methyl-1H-indol-4-yl)-4-morpholinothieno[3,2-d]pyrimidin-6-yl)methyl)piperazin-1-yl)propanamide (10). The title compound was prepared from **32** and 2-methyl-4-(4,4,5,5-tetramethyl-[1,3,2]dioxaborolan-2-yl)-1H-indole (see Supporting Information for procedure) in a manner similar to the Suzuki procedure described for compound **1** to give compound **10** as a white solid (0.295 g, 62%). ^{1}H NMR (400 MHz, DMSO-d_6) δ 8.00 (d, J = 8 Hz, 1H), 7.37 (s, 1H), 7.32 (d, J = 8 Hz, 1H), 7.09 (Br s, 1H), 7.03 (t, J = 8 Hz, 1H), 7.02 (br s, 1H), 6.90 (br s, 1H), 3.93 (t, J = 5 Hz, 4H), 3.81 (s, 2H), 3.77 (t, J = 5 Hz, 4H), 2.47−2.56 (m, 4H), 2.39 (s, 3H), 1.03 (s, 6H). LCMS RT 5.17 min; m/z 534.7 [M + H]$^+$. Analytical LC-MS on a Waters Micromass (ZQ2000), using a 3 mm × 100 mm Higgins Clipeus 5 μm C18 analytical column and H$_2$O/MeCN modified with 0.1% formic acid running a linear gradient from 5% MeCN to 95% MeCN monitoring by DAD UV (200−600 nm) detection and ESI+ TIC MS showed 99% purity.

2-Methyl-2-(4-((2-(1-methyl-1H-indol-4-yl)-4-morpholinothieno[3,2-d]pyrimidin-6-yl)methyl)piperazin-1-yl)propanamide (11). The title compound was prepared from **32** in a manner similar to the Suzuki procedure described for compound **9** to give the title compound **11** (113 mg, 62%). ^{1}H NMR (400 MHz, DMSO-d_6) 8.16 (d, J = 8, 1H), 7.57 (d, J = 8, 1H), 7.42 (m, 3H), 7.28 (t, J = 8, 1H), 7.06 (br d, 1H), 6.93 (br d, 1H), 3.99 (m, 4H), 3.86 (m, 9H), 2.56 (br m, 8H), 1.08 (s, 6H). RT: 3.26 min. MS (ESI): m/z (M + H)$^+$ 534.2. Analytical LC-MS on an Agilent (1200/G6140) using a 1.8 μM, 2.1 mm × 30 mm ZORBAX SD-C18 analytical column, 40 °C, 400 μL/min, and H$_2$O/MeCN modified with 0.05% trifluoroacetic acid running a linear gradient from 3% MeCN to 95% MeCN in 10 min, monitoring by UV wavelength 254 nm and ESI+ TIC MS showed 100% purity.

2-Methyl-2-(4-((4-morpholino-2-(1H-pyrrolo[3,2-c]pyridin-4-yl)thieno[3,2-d]pyrimidin-6-yl)methyl)piperazin-1-yl)-propanamide (12). A mixture of 2-[4-(4-morpholin-4-yl-2-(tributylstannanyl)thieno[3,2-d]pyrimidin-6-ylmethyl)piperazin-1-yl]-isobutyramide **38** (150 mg, 0.22 mmol), 1-benzenesulfonyl-4-bromo-1H-pyrrolo[3,2-c]pyridine (90 mg, 0.27 mmol), Pd(PPh$_3$)$_4$ (25 mg, 10 mol %), and CuI (50 mg, 0.25 mmol) in dioxane (2.5 mL) was purged with argon gas and then heated at 140 °C, for 20 min, in a microwave reactor. The reaction mixture was loaded onto an Isolute SCX-2 cartridge, washed with MeOH/DCM, and then eluted with 2 M NH$_3$ in MeOH. The resulting residue was dissolved in IMS/dioxane (1:1 mL) and 12.5 M aqueous NaOH solution (0.1 mL) added. After stirring for 1 h, the reaction mixture was loaded onto an Isolute SCX-2 cartridge, washed with MeOH/DCM, and then eluted with 2 M NH$_3$ in MeOH/DCM. The resulting residue was purified by flash chromatography (Si-PPC, MeOH:DCM, gradient 0:100 to 05:95) to give compound **12** (28 mg, 24%) as a pale-yellow solid. ^{1}H NMR (400 MHz, CDCl$_3$) δ 9.11 (s, 1 H), 8.54 (d, J = 5.6 Hz, 1 H), 7.45 (s, 1 H), 7.41 (dd, J = 3.3, 0.9 Hz, 1 H), 7.38 (dd, J = 5.6, 0.95 Hz, 1 H), 7.36 (d, J = 3.3 Hz, 1 H), 7.10 (d, J = 5.3 Hz, 1 H), 5.25 (d, J = 5.2 Hz, 1 H), 4.10 (t, J = 4.75 Hz, 4 H), 3.91 (t, J = 4.7 Hz, 4 H), 3.85 (s, 2 H), 2.60 (s, 8 H), 1.24 (s, 6 H). LCMS RT 4.86 min; m/z [M + H]$^+$ 521.3. Analytical LC-MS on a Waters Micromass (ZQ2000), using a 3 mm × 100 mm Higgins Clipeus 5 μm C18 analytical column and H$_2$O/MeCN modified with 0.1% formic acid running a linear gradient from 5% MeCN to 95% MeCN monitoring by DAD UV (200−600 nm) detection and ESI+ TIC MS showed 99% purity.

2-Methyl-2-(4-((4-morpholino-2-(1H-pyrrolo[2,3-c]pyridin-4-yl)thieno[3,2-d]pyrimidin-6-yl)methyl)piperazin-1-yl)-propanamide (13). The title compound was prepared from **38** and tert-butyl 4-bromo-1H-pyrrolo[2,3-c]pyridine-1-carboxylate in a manner similar to the Stille procedure described for compound **12** to give compound **13** as a pale-yellow solid (242 mg, 39%). ^{1}H NMR (400 MHz, DMSO-d_6): δ 11.75 (s, 1 H), 9.13 (s, 1 H), 8.81 (s, 1 H), 7.71 (t, J = 2.7 Hz, 1 H), 7.45 (s, 1 H), 7.40−7.37 (m, 1 H), 7.07 (d, J = 3.5 Hz, 1 H), 6.95 (d, J = 3.5 Hz, 1 H), 4.01 (t, J = 4.6 Hz, 4 H), 3.87 (s, 2H), 3.83 (t, J = 4.6 Hz, 4 H), 2.58 (s, 4 H), 2.49 (s, 4 H), 1.10 (s, 6 H). LCMS: RT 4.51 min, m/z [M + H]$^+$ 521.2. Analytical LC-MS on a Waters Micromass (ZQ2000), using a 3 mm × 100 mm Higgins Clipeus 5 μm C18 analytical column and H$_2$O/MeCN modified with 0.1% formic acid running a linear gradient from 5% MeCN to 95%

MeCN monitoring by DAD UV (200−600 nm) detection and ESI+ TIC MS showed 95% purity.

2-Methyl-2-(4-((4-morpholino-2-(1H-pyrrolo[2,3-b]pyridin-4-yl)thieno[3,2-d]pyrimidin-6-yl)methyl)piperazin-1-yl)-propanamide (14). The title compound was prepared from **38** and 4-bromopyrrolo[2,3-b]pyridine-1-carboxylic acid tert-butylester in a manner similar to the Stille procedure described for compound **12** to give compound **14** as a white powder (0.049 g, 20%). ^{1}H NMR (400 MHz, CDCl$_3$) δ 8.93 (s, 1 H), 8.43 (d, J = 5.2 Hz, 1 H), 8.08 (d, J = 5.2 Hz, 1 H), 7.43 (d, J = 2.2 Hz, 2 H), 7.38 (s, 1 H), 7.09 (d, J = 5.2 Hz, 1 H), 5.24 (d, J = 5.2 Hz, 1 H), 4.10 (t, J = 4.7 Hz, 4 H), 3.92 (t, J = 4.7 Hz, 4 H), 3.86 (s, 2 H), 2.65−2.58 (m, 4 H), 1.60−1.55 (m, 4 H), 1.24 (s, 6 H). LCMS: RT 5.07 min, m/z [M + H]$^+$ 521.3. Analytical LC-MS on a Waters Micromass (ZQ2000), using a 3 mm × 100 mm Higgins Clipeus 5 μm C18 analytical column and H$_2$O/MeCN modified with 0.1% formic acid running a linear gradient from 5% MeCN to 95% MeCN monitoring by DAD UV (200−600 nm) detection and ESI+ TIC MS showed 99% purity.

1-((2-(5-Fluoro-1H-indol-4-yl)-4-morpholinothieno[3,2-d]-pyrimidin-6-yl)methyl)-N,N-dimethylpiperidin-4-amine (15). The title compound was prepared from **35** and 1-(tert-butyldimethylsilyl)-5-fluoro-4-(4,4,5,5-tetramethyl-1,3,2-dioxaborolan-2-yl)-1H-indole (see Supporting Information for procedure) in a manner similar to the Suzuki procedure described for compound **9** to give compound **15** (0.753 g, 26%). ^{1}H NMR (400 MHz, DMSO-d_6) δ 11.22 (s, 1H), 7.47−7.40 (m, 2H), 7.36 (s, 1H), 7.03−6.83 (m, 1H), 6.69−6.65 (m, 1H), 3.93−3.90 (m, 4H), 3.84 (s, 2H), 3.81−3.74 (m, 4H), 2.99−2.91 (m, 2H), 2.17 (s, 6H), 2.07 (t, J = 10.7 Hz, 3H), 1.73 (d, J = 11.6 Hz, 2H), 1.49−1.35 (m, 2H). RT: 6.61 min. MS (ESI): m/z (M + H)$^+$ 495.2. Analytical LC-MS on an Agilent (1200/G6140) using a 1.8 μm, 2.1 mm × 30 mm ZORBAX SD-C18 analytical column, 40 °C, 700 μL/min, and H$_2$O/MeCN modified with 0.05% trifluoroacetic acid running a linear gradient from 2% MeCN to 98% MeCN in 30 min, monitoring by UV wavelength 254 nm and ESI+ TIC MS showed 100% purity.

4-(6-((4-(Dimethylamino)piperidin-1-yl)methyl)-4-morpholinothieno[3,2-d]pyrimidin-2-yl)indolin-2-one (16). The title compound was prepared from **39** in a manner similar to the Stille procedure described for compound **12** to give compound **16** as a yellow powder (32 mg, 14%). ^{1}H NMR (400 MHz, DMSO-d_6) δ 10.47 (s, 1H), 7.96 (d, J = 8.1 Hz, 1H), 7.38 (s, 1H), 7.31 (t, J = 7.8 Hz, 1H), 6.92 (d, J = 7.6 Hz, 1H), 3.88−3.99 (m, 6H), 3.76−3.86 (m, 6H), 2.93 (d, J = 11.6 Hz, 2H), 2.16 (s, 6H), 2.06 (t, J = 10.9 Hz, 3H), 1.73 (d, J = 11.6 Hz, 2H), 1.33−1.51 (m, 2H). MS (ESI): m/z (M + H)$^+$ 493.

N,N-Dimethyl-1-((4-morpholino-2-m-tolylthieno[3,2-d]-pyrimidin-6-yl)methyl)piperidin-4-amine (17). The title compound was prepared from **35** in a manner similar to the Suzuki procedure described for compound **9** to give compound **17** as an off-white powder (250 mg, 55%). ^{1}H NMR (DMSO-d_6) δ 8.14−8.25 (m, 2H), 7.32−7.41 (m, 2H), 7.24−7.32 (m, 1H), 3.92−4.03 (m, 4H), 3.72−3.86 (m, 6H), 2.92 (d, J = 11.7 Hz, 2H), 2.40 (s, 3H), 2.16 (s, 6H), 2.05 (t, J = 11.1 Hz, 3H), 1.72 (d, J = 11.3 Hz, 2H), 1.40 (qd, J = 11.8, 3.8 Hz, 2H). MS = 452 [M + H]$^+$.

1-((2-(Imidazo[1,2-a]pyridin-5-yl)-4-morpholinothieno[3,2-d]pyrimidin-6-yl)methyl)-N,N-dimethylpiperidin-4-amine (18). The title compound was prepared from **39** in a manner similar to the Stille procedure described for compound **12** to give compound **18** as a white solid (72 mg, 63%). ^{1}H NMR (400 MHz, CDCl$_3$) δ 9.23 (s, 1 H), 7.95 (dd, J = 8.6, 1.3 Hz, 1 H), 7.77 (d, J = 8.6 Hz, 1 H), 7.75 (d, J = 1.3 Hz, 1 H), 7.35 (s, 1 H), 7.32−7.29 (m, 1 H), 4.07 (t, J = 4.8 Hz, 4 H), 3.91 (t, J = 4.8 Hz, 4 H), 3.84 (s, 2 H), 3.04 (d, J = 11.25 Hz, 2 H), 2.33−2.25 (m, 6 H), 2.21−2.10 (m, 3 H), 1.84 (d, J = 12.5 Hz, 2 H), 1.61 (m, 2 H). LCMS: RT 3.89 min; m/z [M + H]$^+$ 478. Analytical LC-MS on a Waters Micromass (ZQ2000), using a 3 mm × 100 mm Higgins Clipeus 5 μm C18 analytical column and H$_2$O/MeCN modified with 0.1% formic acid running a linear gradient from 5% MeCN to 95% MeCN monitoring by DAD UV (200−600 nm) detection and ESI+ TIC MS showed 95% purity.

N,N-Dimethyl-1-((2-(3-methylisoquinolin-4-yl)-4-morpholinothieno[3,2-d]pyrimidin-6-yl)methyl)piperidin-4-amine (19). The title compound was prepared from **39** in a manner similar to the Suzuki procedure described for compound **9** to give compound **19** (0.0383 g, 14%) as a light-brown foam. ^{1}H NMR (300 MHz, DMSO-d_6) δ 9.29 (s, 1H), 8.09–8.17 (m, 1H), 7.56–7.72 (m, 2H), 7.48–7.54 (m, 1H), 7.37 (s, 1H), 3.86–3.97 (m, 4H), 3.85 (s, 2H), 3.70–3.78 (m, 4H), 2.96 (d, J = 11.68 Hz, 2H), 2.46 (s, 3H), 2.18 (s, 6H), 2.08 (t, J = 10.74 Hz, 3H), 1.92 (s, 3H), 1.75 (d, J = 12.06 Hz, 2H), 1.34–1.52 (m, 2H). MS (ESI): m/z (M + H)$^+$ 503.0.

N,N-Dimethyl-1-((2-(2-methylbenzo[b]thiophen-3-yl)-4-morpholinothieno[3,2-d]pyrimidin-6-yl)methyl)piperidin-4-amine (20). The title compound was prepared from **39** in a manner similar to the Suzuki procedure described for compound **9** to give compound **20** (0.0037 g, 26%) as an off-white foam. ^{1}H NMR (300 MHz, CDCl$_3$) δ 8.28 (dd, J = 1.13, 7.18 Hz, 1H), 7.72–7.81 (m, 1H), 7.23–7.39 (m, 3H), 3.98–4.17 (m, 4H), 3.85–3.92 (m, 4H), 3.83 (d, J = 0.76 Hz, 2H), 3.05 (d, J = 11.71 Hz, 2H), 2.82 (s, 3H), 2.30 (s, 6H), 2.06–2.20 (m, 3H), 1.83 (d, J = 11.71 Hz, 2H), 1.50–1.72 (m, 2H). MS (ESI): m/z (M + H)$^+$ 508.0.

1-((2-(1H-Indazol-3-yl)-4-morpholinothieno[3,2-d]pyrimidin-6-yl)methyl)-N,N-dimethylpiperidin-4-amine (21). The title compound was prepared from **39** and 1-boc-3-bromo-1H-indazole in a manner similar to the Suzuki procedure described for compound **9** to give compound **21** (0.012 g, 9%) as a white solid. ^{1}H NMR (300 MHz, DMSO-d_6) δ ppm 13.37 (br s, 1H), 8.54 (d, J = 8.3 Hz, 1 H), 7.61 (d, J = 8.3 Hz, 1 H), 7.42 (s, 1 H), 7.40 (t, J = 8.3 Hz, 1 H), 7.24 (t, J = 8.3 Hz, 1 H), 3.92–4.13 (m, 4 H), 3.64–3.92 (m, 6 H), 2.96 (d, J = 11.3 Hz, 2 H), 2.08 (t, J = 10.76 Hz, 2 H), 1.78 (d, J = 11.33 Hz, 1 H), 1.45 (q, J = 11.2 Hz, 2 H). MS (ESI): m/z (M + H)$^+$ 477.

1-((2-(1H-Indazol-1-yl)-4-morpholinothieno[3,2-d]pyrimidin-6-yl)methyl)-N,N-dimethylpiperidin-4-amine (22). To a 0 °C solution of indazole (118 mg, 1.0 mmol) in 8 mL of DMF was added sodium hydride (60 mg, 1.5 mmol, 60% dispersion in oil), stirred at 0 °C for 15 min, then 1-((2-chloro-4-morpholinothieno[3,2-d]-pyrimidin-6-yl)methyl)-N,N-dimethylpiperidin-4-amine (**35**) (395 mg, 1.0 mmol) was added, and the reaction mixture heated to 150 °C for 1 h. The cooled reaction mixture was diluted with water, the resulting suspension was filtered, and the collected solids were purified by flash chromatography (from 100% DCM to 20:80 MeOH w/2% ammonium hydroxide/dichloromethane) and the solids were triturated with ethyl acetate, solids filtered and dried in a 50 °C vacuum oven overnight to give compound **22** as a white powder (233 mg, 49%). ^{1}H NMR (400 MHz, DMSO-d_6) δ: 8.68 (dd, J = 8.7, 0.8 Hz, 1H), 8.39 (d, J = 0.8 Hz, 1H), 7.83–7.93 (m, 1H), 7.56 (ddd, J = 8.5, 7.0, 1.1 Hz, 1H), 7.39 (s, 1H), 7.26–7.37 (m, 1H), 3.95–4.09 (m, 4H), 3.77–3.91 (m, 6H), 2.94 (d, J = 11.7 Hz, 2H), 2.17 (s, 6H), 2.07 (t, J = 10.7 Hz, 3H), 1.73 (d, J = 10.9 Hz, 2H), 1.41 (qd, J = 11.9, 4.0 Hz, 2H). MS (ESI): m/z (M + H)$^+$ 478.

1-((2-(1H-Indol-3-yl)-4-morpholinothieno[3,2-d]pyrimidin-6-yl)methyl)-N,N-dimethylpiperidin-4-amine (23). The title compound was prepared from **35** in a manner similar to the Suzuki procedure described for compound **9** to give compound **23** (0.161 g, 27%) as a cream powder. ^{1}H NMR (400 MHz, CDCl$_3$) δ 8.75 (br s, 1H), 8.63–8.70 (m, 1H), 8.13 (d, J = 2.53 Hz, 1H), 7.37–7.44 (m, 1H), 7.26 (s, 3H), 4.05 (d, J = 5.56 Hz, 4H), 3.92 (d, J = 5.05 Hz, 4H), 3.80 (s, 2H), 2.97–3.08 (m, 2H), 2.29 (s, 6H), 2.05–2.20 (m, 3H), 1.77–1.86 (m, 2H), 1.53–1.66 (m, 2H). Elemental analysis: Theory: C, 65.5%; H, 6.77%; N, 17.6%. Found: C, 65.2%; H, 6.68%; N, 17.4%. MS (ESI): m/z (M + H)$^+$ 477.

1-((2-(1H-Indol-1-yl)-4-morpholinothieno[3,2-d]pyrimidin-6-yl)methyl)-N,N-dimethylpiperidin-4-amine (24). The title compound was prepared from **35** in a manner similar to the procedure described for compound **22** to give compound **24** as an off-white powder (157 mg, 33%). ^{1}H NMR (400 MHz, DMSO-d_6) δ 8.78 (d, J = 7.9 Hz, 1H), 8.30 (d, J = 3.8 Hz, 1H), 7.62 (d, J = 7.5 Hz, 1H), 7.36 (s, 1H), 7.25–7.34 (m, 1H), 7.12–7.23 (m, 1H), 6.70 (d, J = 3.8 Hz, 1H), 3.92–4.04 (m, 4H), 3.75–3.87 (m, 6H), 2.93 (d, J = 11.7 Hz, 2H), 2.16 (s, 6H), 2.06 (t, J = 11.1 Hz, 3H), 1.72 (d, J = 11.7 Hz, 2H), 1.40 (qd, J = 11.8, 3.8 Hz, 2H). MS (ESI): m/z (M + H)$^+$ 477.

1-((2-(1H-Benzo[d]imidazol-1-yl)-4-morpholinothieno[3,2-d]pyrimidin-6-yl)methyl)-N,N-dimethylpiperidin-4-amine (25). A mixture of 1-((2-chloro-4-morpholinothieno[3,2-d]pyrimidin-6-yl)-methyl)-N,N-dimethylpiperidin-4-amine (**35**) (50 mg, 0.13 mmol), benzimidazole (32 mg, 0.27 mmol), and concentrated HCl (53 μL, 0.64 mmol) in 1,4-dioxane (1 mL) was subjected to microwave irradiation at 150 °C for 40 min. The reaction mixture was cooled to ambient temperature and loaded onto an Isolute SCX-2 cartridge (2 g). The cartridge was then washed with MeOH, and the desired product was eluted using 2 M NH$_3$ in MeOH. The eluent was collected and concentrated in vacuo. The resultant residue was purified by flash chromatography (Si-PPC, DCM/2 M NH$_3$ in MeOH 100:0 to 98:2 to 95:5 to 90:10) to afford compound **25** as a white solid (38 mg, 63%). ^{1}H NMR (400 MHz, CDCl$_3$) δ 9.04 (s, 1 H), 8.61–8.57 (m, 1 H), 7.86–7.82 (m, 1 H), 7.43–7.31 (m, 2 H), 7.27 (s, 1H), 4.07 (t, J = 4.8 Hz, 4 H), 3.92 (t, J = 4.8 Hz, 4 H), 3.82 (s, 2 H), 3.08–2.99 (m, 2 H), 2.30 (s, 6 H), 2.20–2.10 (m, 3 H), 1.88–1.78 (m, 2 H), 1.66–1.54 (m, 2 H). LCMS: RT = 5.12 min, m/z [M + H]$^+$ 478.2. Analytical LC-MS on a Waters Micromass (ZQ2000), using a 3 mm × 100 mm Higgins Clipeus 5 μm C18 analytical column and H$_2$O/MeCN modified with 0.1% formic acid running a linear gradient from 5% MeCN to 95% MeCN monitoring by DAD UV (200–600 nm) detection and ESI+ TIC MS showed 99% purity.

N,N-Dimethyl-1-((2-(2-methyl-1H-benzo[d]imidazol-1-yl)-4-morpholinothieno[3,2-d]pyrimidin-6-yl)methyl)piperidin-4-amine (26). A mixture of 1-((2-chloro-4-morpholinothieno[3,2-d]pyrimidin-6-yl)methyl)-N,N-dimethylpiperidin-4-amine (**35**) (500 mg, 1.26 mmol), 1,2-diaminobenzene (550 mg, 5.09 mmol), and concentrated HCl (1 mL, 12 mmol) in 1,4-dioxane (10 mL) was heated at 90 °C for 3 days. The reaction mixture was cooled to ambient temperature and loaded onto an Isolute SCX-2 cartridge (25 g). The cartridge was then washed with MeOH, and the desired product was eluted using 2 M NH$_3$ in MeOH. The eluent was collected and concentrated in vacuo. The resultant residue was purified by flash chromatography (Si-PPC, DCM/2 M NH$_3$ in MeOH 100:0 to 98:2 to 95:5 to 90:10 to 80:20) to afford the title compound as a white solid (220 mg, 37%). LCMS: RT = 1.90 min, m/z [M + H]$^+$ 468.4.

A mixture of N-[6-(4-dimethylaminopiperidin-1-ylmethyl)-4-morpholin-4-yl-thieno[3,2-d]pyrimidin-2-yl]benzene-1,2-diamine (80 mg, 0.17 mmol) and triethyl orthoformate (1 mL, 6.0 mmol) in DMF (1 mL) was heated at 150 °C for 6 h. The reaction mixture was cooled to ambient temperature and loaded onto an Isolute SCX-2 cartridge (10 g). The cartridge was then washed with MeOH, and the desired product was subsequently eluted using 2 M NH$_3$ in MeOH. The eluent was collected and concentrated in vacuo. The resultant residue was purified by flash chromatography (Si-PPC, DCM/2 M NH$_3$ in MeOH 100:0 to 98:2 to 95:5) followed by reverse phase HPLC (Phenomenex Luna C18, 20 mM Et$_3$N in water on a gradient of 20 mM Et$_3$N in acetonitrile 95:5 to 2:98) to afford compound **26** as a white solid (20 mg, 24%). ^{1}H NMR (400 MHz, CDCl$_3$) δ 8.09–8.04 (m, 1 H), 7.74–7.68 (m, 1 H), 7.29–7.24 (m, 3 H), 4.08–4.02 (m, 4 H), 3.91–3.86 (m, 4 H), 3.83 (s, 2 H), 3.08–3.00 (m, 2 H), 2.93 (s, 3 H), 2.30 (s, 6 H), 2.21–2.10 (m, 3 H), 1.88–1.79 (m, 2 H), 1.68–1.53 (m, 2 H). LCMS: RT = 4.24 min, m/z [M + H]$^+$ 492.3 Analytical LC-MS on a Waters Micromass (ZQ2000), using a 3 mm × 100 mm Higgins Clipeus 5 μm C18 analytical column and H$_2$O/MeCN modified with 0.1% formic acid running a linear gradient from 5% MeCN to 95% MeCN monitoring by DAD UV (200–600 nm) detection and ESI+ TIC MS showed 99% purity.

2-Methyl-2-(4-((2-(2-methyl-1H-benzo[d]imidazol-1-yl)-4-morpholinothieno[3,2-d]pyrimidin-6-yl)methyl)piperazin-1-yl)propanamide (27). To a microwave vial was added 150 mg of 2-(4-((2-chloro-4-morpholinothieno[3,2-d]pyrimidin-6-yl)methyl)-piperazin-1-yl)-2-methylpropanamide (**32**), 7.7 mg palladium acetate, 17 mg bis(tri-t-butylphosphine)palladium, 68 mg 2-methylbenzimidazole, and 66 mg sodium tert-butoxide. The vial was capped and purged with nitrogen before addition of 2.6 mL of toluene. The reaction was heated for 105 min at 155 °C. The resulting cooled mixture was loaded onto an SCX column, and the column was washed with methanol. The product was eluted with 2 M NH3 in methanol, and

the product fractions were concentrated in vacuo. The residue obtained was purified by reverse phase HPLC to afford 29.3 mg of **27** as a white solid (100% pure). ^{1}H NMR (400 MHz, DMSO) δ 8.12–7.95 (m, 1H), 7.60 (dt, J = 6.6, 2.8 Hz, 1H), 7.44 (s, 1H), 7.32–7.17 (m, 2H), 7.06 (d, J = 3.1 Hz, 1H), 6.94 (d, J = 2.9 Hz, 1H), 4.04–3.93 (m, 4H), 3.88 (s, 2H), 3.84–3.75 (m, 4H), 2.83 (s, 3H), 2.56 (brm, 4H), 2.47 (brm, 4H), 1.08 (s, 6H). LCMS m/z [M + H]$^+$ 535.2.

4-(2-(2-Ethyl-1*H*-benzo[*d*]imidazol-1-yl)-6-((4-(methylsulfonyl)piperazin-1-yl)methyl)thieno[3,2-*d*]pyrimidin-4-yl)morpholine (28). To a microwave vial was added 1 g of 4-(2-chloro-6-((4-(methylsulfonyl)piperazin-1-yl)methyl)thieno[3,2-*d*]-pyrimidin-4-yl)morpholine (**33**), 95 mg of tris(dibenzylideneacetone)-dipalladium(0), 95 mg 2-dicyclohexylphosphino-2′,4′,6′ triisopropylbi-phenyl, 0.36 g 2-ethylbenzimidazole, and 1.51 g cesium carbonate. *N,N*-Dimethylformamide (16.1 mL) was added, and the reaction was heated for 20 min at 145 °C. The reaction was purified by reverse phase HPLC to afford 283.8 mg of **28** as a white solid (99.5% pure). ^{1}H NMR (400 MHz, DMSO) δ 8.04–7.95 (m, 1H), 7.68–7.59 (m, 1H), 7.47 (s, 1H), 7.29–7.20 (m, 2H), 4.03–3.91 (m, 5H), 3.86–3.76 (m, 4H), 3.26 (q, J = 14.9, 7.5 Hz, 3H), 3.17 (br m, 4H), 2.91 (s, 3H), 2.62 (br m, 4H), 1.32 (t, J = 7.4 Hz, 3H). LCMS m/z [M + H]$^+$ 542.

2-(1-((2-(2-Ethyl-1*H*-benzo[*d*]imidazol-1-yl)-4-morpholinothieno[3,2-*d*]pyrimidin-6-yl)methyl)piperidin-4-yl)propan-2-ol (29). A microwave vial was charged with 2-(1-((2-chloro-4-morpholinothieno[3,2-*d*]pyrimidin-6-yl)methyl)piperidin-4-yl)propan-2-ol (**36**) (1.5 g, 3.65 mmol) and 2-ethyl-1*H*-benzo[*d*]-imidazole (0.60 g, 4.1 mmol), XPhos (0.17 g, 0.36 mmol), tris(dibenzylideneacetone)dipalladium (0.17 g, 0.19 mmol), cesium carbonate (2.4 g, 7.4 mmol), and 1,4-dioxane (15 mL). The reaction was sealed and heated in a Biotage microwave at 140 °C for 40 min. The reaction was then filtered through Celite and concentrated. The crude product was purified by flash chromatography (0–10% MeOH gradient in EtOAc) followed by reverse phase HPLC to give the title compound **29** (0.795 g, 42%). ^{1}H NMR (400 MHz, DMSO-d_6) δ 8.00 (m, 1H), 7.65 (m, 1H), 7.42 (s, 1H), 7.25 (m, 2H), 4.07 (s, 1H), 3.97 (m, 4H), 3.83 (s, 2H), 3.81 (m, 4H), 3.27 (m, 2H), 2.99 (d, J = 10.9, 2H), 1.99 (t, J = 11.3, 2H), 1.67 (d, J = 11.3, 2H), 1.32 (t, J = 7.43, 3H), 1.11–1.29 (m, 3H), 1.04 (s, 6H). RT: 7.57 min. MS (ESI): m/z (M + H)$^+$ 521.3. Analytical LC-MS on an Agilent (1200/G6140) using a 1.8 μM, 2.1 mm × 30 mm ZORBAX SD-C18 analytical column, 40 °C, 700 μL/min and H$_2$O/MeCN modified with 0.05% trifluoroacetic acid running a linear gradient from 2% MeCN to 98% MeCN in 30 min, monitoring by UV wavelength 254 nm and ESI+ TIC MS showed 99% purity.

4-(6-((2,2-Dimethyl-4-(oxetan-3-yl)piperazin-1-yl)methyl)-2-(2-ethyl-1*H*-benzo[*d*]imidazol-1-yl)thieno[3,2-*d*]pyrimidin-4-yl)morpholine (30). A mixture of 2-chloro-6-(2,2-dimethyl-4-oxetan-3-ylpiperazin-1-ylmethyl)-4-morpholin-4-yl-thieno[3,2-*d*]pyrimidine (**37**) (136 mg, 0.31 mmol), 2-ethylbenzimidazole (48 mg, 0.33 mmol), tris(dibenzylideneacetone)dipalladium (8 mg, 3 mol %), XPhos (14 mg, 9 mol %), and Cs$_2$CO$_3$ (143 mg, 0.44 mmol) in DMF (4 mL) was purged with argon then heated at 150 °C for 30 min in a microwave reactor. The reaction mixture was loaded onto an Isolute SCX-2 cartridge which was washed with MeOH and the product eluted with 2 M NH$_3$/MeOH. The resulting residue was purified by column chromatography (Si-PCC, MeOH/DCM, 0–5%) then (Si-PCC, 2 M NH$_3$/MeOH/DCM, 0–2%) affording the **30** as a cream solid (45 mg, 26%). ^{1}H NMR (400 MHz, CDCl$_3$) δ 7.97–7.96 (1 H, m), 7.75–7.74 (1 H, m), 7.32–7.22 (3 H, m), 4.66 (2 H, t, J = 6.47 Hz), 4.59 (2 H, t, J = 6.08 Hz), 4.04 (4 H, t, J = 4.72 Hz), 3.91–3.86 (6 H, m), 3.46–3.45 (1 H, m), 3.33 (2 H, q, J = 7.48 Hz), 2.64 (2 H, t, J = 4.98 Hz), 2.33 (2 H, s), 2.14 (2 H, s), 1.42 (3 H, t, J = 7.47 Hz), 1.20 (6 H, s). LCMS: RT 2.78 min; m/z [M + H]$^+$ 548.3. Analytical LC-MS on a Waters Micromass (ZQ2000), using a 100 mm × 2.1 mm Acquity BEH C18 1.7 μM analytical column and H$_2$O/MeOH modified with 0.1% formic acid running a linear gradient from 5% to 95% MeOH monitoring by PDA UV detection and ESI+ TIC MS showed 94% purity.

Characterization of Biochemical and Cellular Activity. In vitro enzymatic activity of the class I PI3K isoforms was measured

using a fluorescence polarization assay that monitors formation of the product 3,4,5-inositoltriphosphate molecule as it competes with fluorescently labeled PIP3 for binding to the GRP-1 pleckstrin homology domain protein. An increase in phosphatidyl inositide-3-phosphate product results in a decrease in fluorescence polarization signal as the labeled fluorophore is displaced from the GRP-1 protein binding site. Class I PI3K isoforms were purchased from Millipore or were expressed and purified as heterodimeric recombinant proteins. Tetramethylrhodamine-labeled PIP3 (TAMRA-PIP3), di-C8-PIP2, and PIP3 detection reagents were purchased from Echelon Biosciences. PI3K isoforms were assayed under initial rate conditions in the presence of 10 mM Tris (pH 7.5), 25 μM ATP, 9.75 μM PIP2, 5% glycerol, 4 mM MgCl$_2$, 50 mM NaCl, 0.05% (v/v) Chaps, 1 mM dithiothreitol, and 2% (v/v) DMSO at the following concentrations for each isoform: PI3Kα,β at 60 ng/mL; PI3Kγ at 8 ng/mL; PI3Kδ at 45 ng/mL. After assay for 30 min at 25 °C, reactions were terminated with a final concentration of 9 mM EDTA, 4.5 nM TAMRA-PIP3, and 4.2 μg/mL GRP-1 detector protein before reading fluorescence polarization on an Envision plate reader. IC$_{50}$ or K_i apparent values were calculated by fitting the dose–response curves to a four-parameter equation or Morrison tight-binding equation for competitive inhibitors, respectively. All data points are an average of a minimum of three runs.

The human B-cell line, Ri-1, was plated in 384-well tissue culture plates in RPMI1640. Test compound was added to replicate wells with a final DMSO concentration not to exceed 0.5%. After 30 min, cells were treated with 25 μg/mL F(ab′)2 Frag Goat antihuman IgM Fc5u (Jackson 109−006−129) for 1 h at 37 °C with 5% CO$_2$. Following all treatments, cells were lysed in lysis buffer supplemented with phosphatase and protease inhibitors under nondenaturing conditions at 4 °C. Quantitative levels of pAkt Ser473 protein lysates were measured using Meso Scale Discovery (MSD cat. no. K1211CAD) electrochemiluminescence technology. Briefly, MSD Multi-Spot pAkt Ser473 384-well plates were blocked with 35 mL of 5% BSA blocking buffer for 60 min at room temperature (RT) and washed four times in Tris wash buffer. The plates were incubated with 35 mL of pAkt Ser473/protein lysate on the plate shaker overnight at 4 °C. Plates were then washed with Tris wash buffer four times. The wells were then incubated with 10 mL of detection antibody per well for 2 h on the shaker at RT. Plates were then washed again with Tris wash buffer four times after, and 35 mL of read buffer was added and the plates were read using a MSD Sector Imager 6000. All data points are an average of a minimum of three runs.

Computational Methods. The sequences of the kinase domains of the four PI3K isoforms from multiple species were aligned using PSI-BLAST (NCBI). A human PI3K.α H1047R mutant structure (PDB code 3HIZ) was chosen as the template because, among all structures available then, it shared with human PI3Kδ the highest level of sequence homology both overall and around the active site. Sequence alignment was manually refined before a model of human PI3Kδ was built using PRIME (Schrödinger) with standard parameters. Subsequently, a mouse PI3Kδ structure (PDB 2WXP) was published. The structure supported the previous homology model and was adopted for the docking calculation. Structure of the target protein was processed using Maestro (Schrödinger). Ligands were prepared using LigPrep (Schrödinger) and docked against the target using GLIDE (Schrödinger) in SP or XP modes. Torsional angle analysis was carried out as described. Substructures representing the torsional angles in question were minimized at molecular mechanics (MacroModel, Schrödinger) and then at quantum mechanics level (Jaguar, Schrödinger). The resulting conformer was used to perform a "relaxed coordinate scan" of the dihedral in 15° increment using density functional theory (B3LYP) with 6-31G** basis set (Jaguar, Schrödinger).

ASSOCIATED CONTENT

S Supporting Information

Characterization of synthetic intermediates and compounds **32–39**. This material is available free of charge via the Internet at http://pubs.acs.org.

AUTHOR INFORMATION

Corresponding Author

*Phone: (650) 467-7450. Fax: (650) 467-8922. E-mail: bsafina@gene.com.

Notes

The authors declare no competing financial interest.

ACKNOWLEDGMENTS

REFERENCES

(1) Isaacs, J. D. The changing face of rheumatoid arthritis: sustained remission for all? *Nature Rev. Immunol.* **2010**, *10*, 605–611.

(2) Majithia, V.; Geraci, S. A. Rheumatoid Arthritis: Diagnosis and Management. *Am. J. Med.* **2007**, *120*, 936–939.

(3) Van Vollenhoven, R. F. Treatment of rheumatoid arthritis: state of the art 2009. *Nature Rev. Rheum.* **2009**, *5*, 531–541.

(4) Allison, M. PML problems loom for Rituxan. *Nature Biotechnol.* **2010**, *28*, 105–106.

(5) Cantley, L. C. The phosphoinositide 3-kinase pathway. *Science* **2002**, *296*, 1655–1657.

(6) Rommel, C.; Camps, M.; Ji, H. PI3Kδ and PI3Kγ: partners in crime in inflammation in rheumatoid arthritis and beyond? *Nature Rev. Immunol.* **2007**, *7*, 191–201.

(7) (a) Clayton, E.; Bardi, G.; Bell, S. E.; Chantry, D.; Downes, C. P.; Gray, A.; Humphries, L. A.; Rawlings, D.; Reynolds, H.; Vigorito, E.; Turner, M. A Crucial Role for the p110δ Subunit of Phosphatidylinositol 3-Kinase in B Cell Development and Actication. *J. Exp. Med.* **2002**, *196*, 753–763. (b) Jou, S.; Carpino, N.; Takahashi, Y.; Piekorz, R.; Chao, J.; Carpino, N.; Wang, D.; Ihle, J. N. Essential,

Nonredundant Role for the Phosphoinositide 3-Kinase p110δ in Signaling by the B-Cell Receptor Complex. *Mol. Cell. Biol.* **2002**, *22*, 8580–8591. (c) Okkenhaug, K.; Bilancio, A.; Farjot, G.; Priddle, H.; Sancho, S.; Peskett, E.; Pearce, W.; Meek, S. E.; Salpekar, A.; Waterfield, M. D.; Smith, A. J. H.; Vanhaesebroeck, B. Impaired B and T Cell Antigen Receptor Signaling in p110δ PI 3-Kinase Mutant Mice. *Science* **2002**, *297*, 1031–1034.

(8) Edwards, C. W. J. Cambridge, G. B-cell targeting in rheumatoid arthritis and other autoimmune disease. *Nature Rev. Immunol.* **2006**, *6*, 394–403.

(9) Monach, P. A.; Benoist, C.; Mathis, D. The Role of Antibodies in Mouse Models of Rheumatoid Arthritis, and Relevance to Human Disease. *Adv. Immunol.* **2004**, *82*, 217–248.

(10) Vanhaesebroeck, B.; Ali, K.; Bilancio, A.; Geering, B.; Foukas, L. C. Signalling by PI3K isoforms: insights from gene-targeted mice. *Trends Biochem. Sci.* **2005**, *30*, 194–204.

(11) Rückle, T.; Schwarz, M. K.; Rommel, C. PI3Kγ inhibition: towards an 'aspirin of the 21st century'? *Nature Rev. Drug Discovery* **2006**, *5*, 903–918.

(12) (a) Ameriks, M. K.; Venable, J. D. Small Molecule Inhibitors of Phosphoinositide 3-Kinase (PI3K) δ and γ. *Curr. Top. Med. Chem.* **2009**, *9*, 738–753. (b) Herman, S. E. M.; Gordon, A. L.; Wagner, A. J.; Heerema, N. A.; Zhao, W.; Flynn, J. M.; Jones, J.; Andritsos, L.; Puri, K. D.; Lannutti, B. J.; Giese, N. G.; Zhang, X.; Wei, L.; Byrd, J. C.; Johnson, A. J. The phosphatidylinositol 3-kinase-δ inhibitor CAL-101 demonstrates promising pre-clinical activity in chronic lymphoctic leukemia by antagonizing intrinsic and extrinsic cellular survival signals. *Blood* **2010**, *116*, 2078–2087. (c) Williams, O.; Houseman, B. T.; Kunkel, E. J.; Aizenstein, B.; Hoffman, R.; Knight, Z. A.; Shokat, K. M. Discovery of Dual Inhibitors of the Immune Cell PI3Ks p110δ and p110γ: A Prototype for New Anti-inflammatory Drugs. *Chem. Biol.* **2010**, *17*, 123–134.

(13) Berndt, A.; Miller, S.; Williams, O.; Le, D. D.; Houseman, B. T.; Pacold, J. I.; Gorrec, F.; Hon, W.; Liu, Y.; Rommel, C.; Gaillard, P.; Rückle, T.; Schwarz, M. K.; Shokat, K. M.; Shaw, J. P.; Williams, R. L. The p110δ structure: mechanisms for selectivity and potency of new PI(3)K inhibitors. *Nature Chem. Biol.* **2010**, *6*, 117–124.

(14) Sutherlin, D. P.; Sampath, D.; Berry, M.; Castanedo, G.; Chang, Z.; Chuckowree, I.; Dotson, J.; Folkes, A.; Friedman, L.; Goldsmith, R.; Heffron, T.; Lee, L.; Lesnick, J.; Lewis, C.; Mathieu, S.; Nonomiya, J.; Olivero, A.; Pang, J.; Prior, W. W.; Salphati, L.; Sideris, S.; Tian, Q.; Tsui, V.; Wan, N. C.; Wang, S.; Wiesmann, C.; Wong, S.; Zhu, B.-Y. Discovery of (Thienopyrimidine-2-yl)aminopyrimidines as Potent, Selective, and Orally Available Pan-PI3-Kinase and Dual Pan-PI3-Kianse/mTOR Inhibitors for the Treatment of Cancer. *J. Med. Chem.* **2010**, *53*, 1086–1097.

(15) Bode, C. The nasty surprise of a complex drug–drug interaction. *Drug Discovery Today* **2010**, *15*, 391–395.

(16) (a) Venkatakrishnan, K.; Obach, R. S. Drug–Drug Interactions via Mechanism-Based Cytochrome P450 Inactivation: Points to Consider for Risk Assessment from in Vitro Data and Clinical Pharmacologic Evaluation. *Curr. Drug Metab.* **2007**, *8*, 449–462. (b) Riley, R. J.; Grime, K.; Weaver, R. Time-Dependent CYP inhibition. *Expert Opin. Drug Metab. Toxicol.* **2007**, *3*, 51–66.

(17) (a) Walsh, J. S.; Miwa, G. T. Bioactivation of Drugs: Risk and Drug Design. *Annu. Rev. Pharmacol. Toxicol.* **2011**, *51*, 145–167. (b) Kalgutkar, A. S.; Obach, R. S.; Maurer, T. S. Mechanism-Based Inactivation of Cytochrome P450 Enzymes: Chemical Mechansims, Structure–Activity Relationships and Relationship to Clinical Drug–Drug Interactions and Idiosyncratic Adverse Drug Reactions. *Curr. Drug Metab.* **2007**, *8*, 407–447.

(18) (a) Obach, R. S.; Walsky, R. L.; Venkatakrishnan, K. Mechanism-Based Inactivation of Human Cytochrome P450 Enzymes and the Prediction of Drug–Drug Interactions. *Drug Metab. Dispos.* **2006**, *35*, 246–255. (b) Zimmerlin, A.; Trunzer, M.; Faller, B. CYP3A Time-Dependent Inhibition Risk Assessment Validated with 400 Reference Drugs. *Drug Metab. Dispos.* **2011**, *39*, 1039–1046. (c) Krippendorff, B.-F.; Neuhaus, R.; Lienau, P.; Reichel, A.; Huisinga, W. Mechanism-Based Inhibition: Deriving KI and kinact

Directly form Time-Dependent IC$_{50}$ Values. *J. Biomol. Screening* **2009**, *14*, 913−923. (d) BurtH. J.GaletinA.HoustonJ. B.IC$_{50}$-based approaches as an alternative method for assessment of time-dependent inhibition of CYP3A4 *Xenobiotica* **2010**, *40*, 331−343. (e) Mukadam, S.; Tay, S.; Tran, D.; Wang, L.; Delarosa, E. M.; Khojasteh, S. C.; Halladay, J. S.; Kenny, J. R. Evaluation of Time-Dependent Cytochrome P450 Inhibition in a High-Troughput, Automated Assay: Introducing a Novel Area Under the Curve Shift Approach. *Drug Metab. Lett.* **2012**, *6*, 43−53.

(19) (a) Raynaud, F. I.; Eccles, S. A.; Patel, S.; Alix, S.; Box, G.; Chuckowree, I.; Folkes, A.; Gowan, S.; De haven Brandon, A.; Di Stefano, F.; Hayes, A.; Henley, A. T.; Lensun, L.; Pergl-Wilson, G.; Robson, A.; Saghir, N.; Zhyvoloup, A.; McDonald, E.; Sheldrake, P.; Shuttleworth, S.; Valenti, M.; Wan, N. C.; Clarke, P. A.; Workman, P. Biological properties of potent inhibitors of class I phosphatidylinositide 3-kinase: from PI-103 through PI-540, PI-620 to the oral agent GDC-0941. *Mol. Cancer Ther.* **2009**, *8*, 1725−1738. (b) Folkes, A. J.; Ahmadi, K.; Alderton, W. K.; Alix, S.; Baker, S. J.; Box, G.; Chuckowree, I. S.; Clarke, P. A.; Depledge, P.; Eccles, S. A.; Friedman, L. S.; Hayes, A.; Hancox, T. C.; Kugendradas, A.; Lensun, L.; Moore, P.; Olivero, A. G.; Pang, J.; Patel, S.; Pergl-Wilson, G. H.; Raynaud, F. I.; Robson, A.; Saghir, N.; Salphati, L.; Sohal, S.; Ultsch, M. H.; Valenti, M.; Wallweber, H. J. A.; Wan, N. C.; Wiesmann, C.; Workman, P.; Zhyvoloup, P.; Zvelebil, M. J.; Shuttleworth, S. J. The identification of 2-(1*H*-indazol-4-yl)-6-(4-methanesulfonyl-piperazin-1-ylmethyl)-4-morpholin-4-yl-thieno-[3,2-*d*]pyrimidine (GDC-0941) as a potent, selective, orally bioavailable inhibitor of class I PI3 kinase for the treatment of cancer. *J. Med. Chem.* **2008**, *51*, 5522−5532.

(20) Sweeney, Z. K.; Murray, J.; Chan, B. K.; Balazs, M.; Bradley, E.; Castanedo, G.; Chabot, C.; Chantry, D.; Flagella, M.; Goldstein, D. M.; Kondru, R.; Lesnick, J.; Li, J.; Lucas, M. C.; Nonomiya, J.; Pang, J.; Price, S.; Salphati, L.; Safina, B.; Savy, P. P. A.; Seward, E. M.; and Sutherlin, D. P. unpublished results.

(21) Jamei, M.; Marciniak, S.; Feng, K.; Barnett, A.; Tucker, G.; Rostami-Hodjegan, A. The Simcyp Population-Based ADME Simulator. *Exp. Opin. Drug Metab. Toxicol.* **2009**, *5*, 211−223.

(22) (a) Chen, A.; Dubé, D.; Dubé, L.; Gagné, S.; Gallant, M.; Gaudreault, M.; Grimm, E.; Houle, R.; Lacombe, P.; Laliberté, S.; Liu, S.; MacDonald, D.; Mackay, B.; Martin, D.; McKay, D.; Powell, D.; Lévesque, J.-F. *Bioorg. Med. Chem. Lett.* **2010**, *20*, 5074−5079. (b) Walsh, J. S.; Miwa, G. T. *Annu. Rev. Pharmacol. Toxicol.* **2011**, *51*, 145−167.

(23) (a) Dalvie, D. K.; Kalgutkar, A. S.; K-Bakht, S. C.; Obach, R. S.; O'Donnell, J. P. Biotransformation Reactions of Five-Membered Aromatic Heterocyclic Rings. *Chem. Res. Toxicol.* **2002**, *15*, 269−299. (b) Argikar, U. A.; Mangold, J. B.; Harriman, S. P. Strategies and Chemical Design Approaches to Reduce the Potential for Formation of Reactive Metabolic Species. *Curr. Top. Med. Chem.* **2011**, *11*, 419−449.

(24) (a) Guengerich, F. P. Mechanism of Cytochrome P450 Substrate Oxidation: MiniReview. *J. Biochem. Mol. Toxicol.* **2007**, *21*, 163−168. (b) Ortiz de Montellano, P. R. *Chem. Rev.* **2010**, *110*, 932−948.

(25) Milletti, F.; Storchi, L.; Sforna, G.; Cruciani, G. New and original pK_a prediction method using grid molecular interaction fields. *J. Chem. Inf. Model.* **2007**, *47*, 2172−2181.

(26) Benchware 3D Explorer (v2.6, Tripos).